LI
LABORATORY INVESTIGATION
THE BASIC AND TRANSLATIONAL PATHOLOGY RESEARCH JOURNAL
VOLUME 99 | SUPPLEMENT 1 | MARCH 2019

USCAP 2019

ABSTRACTS

TECHNIQUES (INCLUDING ULTRASTRUCTURE) (1978-2008)

USCAP 108TH ANNUAL MEETING

UNLOCKING YOUR INGENUITY

MARCH 16-21, 2019

National Harbor, Maryland
Gaylord National Resort & Convention Center

Published by
SPRINGER NATURE
www.ModernPathology.org

USCAP Creating a Better Pathologist
AN OFFICIAL JOURNAL OF THE UNITED STATES AND CANADIAN ACADEMY OF PATHOLOGY

EDUCATION COMMITTEE

Jason L. Hornick, Chair
Rhonda K. Yantiss, Chair, Abstract Review Board and Assignment Committee
Laura W. Lamps, Chair, CME Subcommittee
Steven D. Billings, Interactive Microscopy Subcommittee
Shree G. Sharma, Informatics Subcommittee
Raja R. Seethala, Short Course Coordinator
Ilan Weinreb, Subcommittee for Unique Live Course Offerings
David B. Kaminsky (Ex-Officio)
Aleodor (Doru) Andea
Zubair Baloch
Olca Basturk
Gregory R. Bean, Pathologist-in-Training
Daniel J. Brat
Ashley M. Cimino-Mathews
James R. Cook
Sarah M. Dry
William C. Faquin
Carol F. Farver
Yuri Fedoriw
Meera R. Hameed
Michelle S. Hirsch
Lakshmi Priya Kunju
Anna Marie Mulligan
Rish Pai
Vinita Parkash
Anil Parwani
Deepa Patil
Kwun Wah Wen, Pathologist-in-Training

ABSTRACT REVIEW BOARD

Benjamin Adam
Michelle Afkhami
Narasimhan (Narsi) Agaram
Rouba Ali-Fehmi
Ghassan Allo
Isabel Alvarado-Cabrero
Christina Arnold
Rohit Bhargava
Justin Bishop
Jennifer Boland
Elena Brachtel
Marilyn Bui
Shelley Caltharp
Joanna Chan
Jennifer Chapman
Hui Chen
Yingbei Chen
Benjamin Chen
Rebecca Chernock
Beth Clark
James Conner
Alejandro Contreras
Claudiu Cotta
Timothy D'Alfonso
Farbod Darvishian
Jessica Davis
Heather Dawson
Elizabeth Demicco
Suzanne Dintzis
Michelle Downes
Daniel Dye
Andrew Evans
Michael Feely
Dennis Firchau
Larissa Furtado
Anthony Gill
Ryan Gill
Paula Ginter
Tamara Giorgadze
Raul Gonzalez
Purva Gopal
Anuradha Gopalan
Jennifer Gordetsky
Rondell Graham
Alejandro Gru
Nilesh Gupta
Mamta Gupta
Krisztina Hanley
Douglas Hartman
Yael Heher
Walter Henricks
John Higgins
Mai Hoang
Mojgan Hosseini
Aaron Huber
Peter Illei
Doina Ivan
Wei Jiang
Vickie Jo
Kirk Jones
Neerja Kambham
Chiah Sui (Sunny) Kao
Dipti Karamchandani
Darcy Kerr
Ashraf Khan
Rebecca King
Michael Kluk
Kristine Konopka
Gregor Krings
Asangi Kumarapeli
Alvaro Laga
Cheng-Han Lee
Zaibo Li
Haiyan Liu
Xiuli Liu
Yan-Chun Liu
Tamara Lotan
Anthony Magliocco
Kruti Maniar
Jonathan Marotti
Emily Mason
Jerri McLemore
Bruce McManus
David Meredith
Anne Mills
Neda Moatamed
Sara Monaco
Atis Muehlenbachs
Bita Naini
Dianna Ng
Tony Ng
Ericka Olgaard
Jacqueline Parai
Yan Peng
David Pisapia
Alexandros Polydorides
Sonam Prakash
Manju Prasad
Peter Pytel
Joseph Rabban
Stanley Radio
Emad Rakha
Preetha Ramalingam
Priya Rao
Robyn Reed
Michelle Reid
Natasha Rekhtman
Michael Rivera
Michael Roh
Andres Roma
Avi Rosenberg
Esther (Diana) Rossi
Peter Sadow
Safia Salaria
Steven Salvatore
Souzan Sanati
Sandro Santagata
Anjali Saqi
Frank Schneider
Jeanne Shen
Jiaqi Shi
Wun-Ju Shieh
Gabriel Sica
Deepika Sirohi
Kalliopi Siziopikou
Lauren Smith
Sara Szabo
Julie Teruya-Feldstein
Gaetano Thiene
Khin Thway
Rashmi Tondon
Jose Torrealba
Evi Vakiani
Christopher VandenBussche
Sonal Varma
Endi Wang
Christopher Weber
Olga Weinberg
Sara Wobker
Mina Xu
Shaofeng Yan
Anjana Yeldandi
Akihiko Yoshida
Gloria Young
Minghao Zhong
Yaolin Zhou
Hongfa Zhu
Debra Zynger

1978 Mismatch Repair Protein (MMR) Immunohistochemistry (IHC) in Cases of Recurrent Gynecologic and Gastrointestinal Malignancies: Is There a Need for Repeat IHC Staining?

John Aird[1], Michael Steel[2], Robert Wolber[3], Lynn Hoang[2], David Schaeffer[1]
[1]Vancouver General Hospital, Vancouver, BC, [2]University of British Columbia, Vancouver, BC, [3]University of British Columbia, North Vancouver, BC

Disclosures: John Aird: None; Michael Steel: None; Robert Wolber: None; Lynn Hoang: None; David Schaeffer: None

Background: In recent years, the National Cancer Comprehensive Network (NCCN) has allowed for the use of immune checkpoint inhibitors, such as Pembrolizumab, for the treatment of recurrent/progressive malignancies which fail to respond to prior cytotoxic therapy. This has been endorsed in a variety of tumor types, including endometrial, tubo-ovarian, colonic and pancreatic carcinoma. As a result, there have been increased requests by oncologists to re-test metastatic/recurrent tumors for MMR proteins, despite testing having already been done on the original tumor. It remains unclear however, whether there is any benefit in re-testing patients. The aim of our study was to compare MMR staining patterns in primary and metastatic/recurrent tumors in a large health care region and document any changes in MMR staining pattern.

Design: Using the pathology laboratory database encompassing 3 hospitals, we identified patients who had MMR immunohistochemistry performed on their primary neoplasm and who also had a recurrence of their cancer confirmed by tissue biopsy. We compared the MMR IHC profile on the original tumor to their recurrences. An additional 32 cases of recurrent endometrial carcinoma from a prior study (spanning 1985-2009, PMID: 28061006) were also included.

Results: From 2011-2016, a total of 4525 cases had MMR IHC done on the primary tumor (2661 colonic, 34 small bowel, 69 pancreatic, 17 biliary, 57 gastric, 7 appendiceal, 1446 endometrial, 112 ovarian, 7 ureteric, 111 skin, 4 other site). Approximately 343 (7.6%) had a tissue sampling showing metastatic/recurrent disease. Using the primary series and additional cases, 29/4557 had MMR staining repeated on the recurrent tumor (Table 1). 28 cases had identical MMR staining patterns to the primary neoplasm. One patient with endometrioid adenocarcinoma had a normal MMR profile on the primary tumor but a loss of MLH1/PMS2 on a soft tissue recurrence 2 years later.

Primary Site	Colorectal	Small Bowel	Endometrium	Ovary	Skin
Number	19	1	6	1	2
MMR IHC Profile	13	1	4	1	0
Normal	5	0	2	0	0
MLH1/PMS2 Loss	1	0	0	0	2
MSH2/MSH6 Loss	0	0	0	0	0
Isolated MSH6 Loss	0	0	0	0	0
Isolated PMS2 Loss					

Conclusions: Concordance of MMR staining patterns in primary and recurrent tumor was seen in 97% of cases. Only one case showed a change in MMR staining profile from normal to MLH1/PMS2 lost. Ongoing work is being done to evaluate MMR on all the tissue recurrences as well as synchronous tumors to better determine how many tumors change MMR staining patterns with disease progression/treatment and how this affects patients' options for immune checkpoint inhibitors.

1979 Abstract Withdrawn

1980 Cesarean-Induced Isthmoceles: To See or Not to See - A Question of Dissection

Brooke Bertus[1], Joshua Shrout[1], Colin Winkie[2], Haydon Bennett[1], Jose Garza-Leal[3], James Coad[1]
[1]West Virginia University, Morgantown, WV, [2]West Virginia University, Bridgeport, WV, [3]Universidad Autónoma de Nuevo León Facultad de Medicina, Monterrey, NL, Mexico

Disclosures:
Brooke Bertus: None; Joshua Shrout: None; Colin Winkie: None; Haydon Bennett: None; Jose Garza-Leal: None; James Coad: None

Background: Increasingly, cesarean delivery-induced isthmoceles are being associated with abnormal uterine bleeding, pelvic pain, secondary infertility and other conditions. Isthmoceles result from suboptimal C-section healing that leads to an anterior lower uterine segment (*LUS*) endometrial out-pouching (*isthmocele*) with wall thinning. Well-suited for most diagnostic assessments, uterine specimens

are traditionally bivalved in the frontal/coronal plane. As this approach does not provide a longitudinal cross-sectional view of the LUS, it limits the evaluation for C-section associated changes. This study's purpose was to assess the utility of a midline sagittal dissection method when assessing for such changes.

Design: One-hundred premenopausal patients with a cesarean delivery history were assessed using a midline sagittal section through the LUS. The presence or absence of macroscopic C-section related changes was documented.

Results: Women included in this study were 41 ± 6 years of age and had a median of 2 prior cesarean deliveries (*range: 1-4 deliveries*). The uteri weighed 133 ± 49 g and sounded 8.1 ± 0.9 cm. Upon sagittal section examination, 99 uteri had a grossly identifiable C-section scar(*s*). 2 had intact transmural incisional healing (*complete union healing*). 80 had isolated inner nonunion healing with variably prominent cesarean-induced isthmocele formation. 4 had isolated outer nonunion healing without isthmocele formation. 11 had both inner and outer nonunion healing. 2 had complete transmural nonunion healing with localized loss of LUS wall integrity. Inner and outer nonunion healing, when present, involved on average 39 ± 22% (*median 40%*) and 25 ± 16% (*median 20%*) of the wall thickness, respectively. Due to the nonunion healing, the resultant wall thickness at the C-section site was 5.5 ± 2.5 mm. When compared to the adjacent uterine wall, this resulted in an approximately 69 ± 15% thinner wall. 2 isthmoceles each contained either an endometrial or endocervical-type polyp.

Figure 1 - 1980

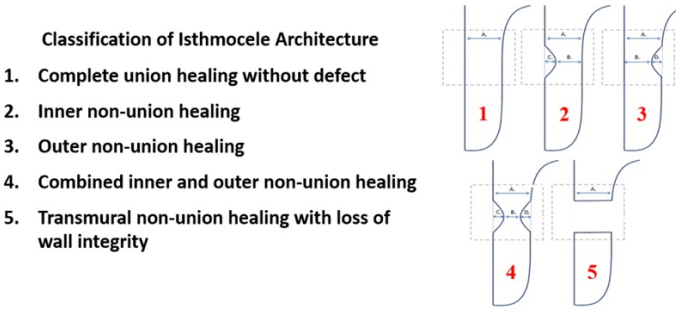

Figure 2 - 1980

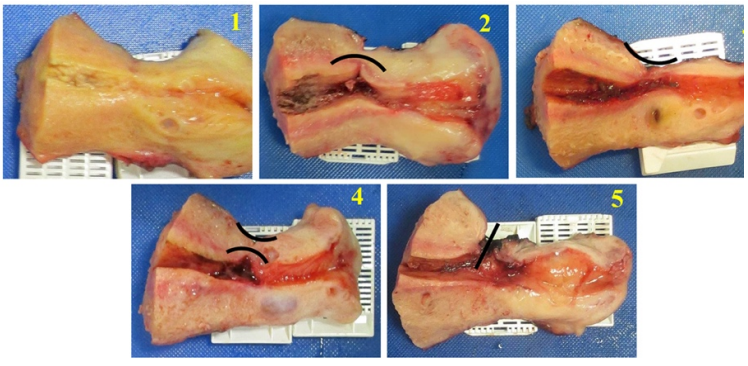

Conclusions: Cesarean delivery-associated changes were identified in 99% of the subject's uteri, including various patterns of suboptimal healing-related changes. The inclusion of a midline sagittal LUS section during uterine dissection enhances the detection of C-section related changes, including the identification of isthmoceles and polyps.

1981 PD-L1 in Breast Cancer: 3 Different Scoring Systems

Dina Boles[1], Elzbieta Slodkowska[1], Katarzyna J. Jerzak[2], Ellen Warner[3], Siqi Zhu[4], Gregory Pond[5], Sharon Nofech-Mozes[1]
[1]Sunnybrook Health Sciences Centre - University of Toronto, Toronto, ON, [2]Sunnybrook Odette Cancer Centre, Toronto, ON, [3]Odette Cancer Center, Toronto, ON, [4]Sunnybrook Research Institute, Toronto, ON, [5]McMaster University, Hamilton, ON

Disclosures: Dina Boles: None; Elzbieta Slodkowska: None; Katarzyna J. Jerzak: None; Ellen Warner: None; Siqi Zhu: None; Gregory Pond: None; Sharon Nofech-Mozes: None

Background: Programmed cell death ligand 1 (PD-L1) is a major immune checkpoint protein that mediates antitumor immune suppression and response. Antibodies directed against PD-1 or its ligand (PD-L1) provide disease control in different cancers. Standardized scoring criteria (SC) for PD-L1 have been identified for lung and bladder cancers, but are not yet standardized for breast cancer (BC). Clinical trials (CTL) with pembrolizumab (Keynote CTL), atezolizumab (IMpassion130 CTL) and avelumab (JAVELIN CTL) among women with metastatic BC have shown increased overall response rates in PD-L1 positive as opposed to PD-L1 negative tumors using different SC. In this study, we compared 3 sets of criteria for scoring PD-L1 expression in BC.

Design: We studied 95 BCs from women ≤ 40 by immunohistochemistry (IHC) on tissue microarrays from 68 resections pre-adjuvant systemic therapy (NAT) and 27 whole sections from core biopsies pre-NAT. Slides were evaluated by 2 pathologists using clone 22C3 on DAKO Omnis for membranous labeling (any intensity) in tumor cells (TC) or cytoplasmic in immune/stromal cells (IC) following 3 sets of SC (table 1). The proportion of PD-L1 positive cases by each set of criteria was evaluated. Prognostic associations of scoring results with recurrence free survival (RFS) were then computed using univariate and multivariate Cox regression models.

Results: PD-L1 was scored positive in 16 cases (16.8%) with only 1 high expressor (HEx) using SC1, 47 cases (49.4 %) with SC2 and 43 cases (45.2%) with SC3 (30 were HEx). In this cohort, SC2 and SC3 were highly concordant for PD-L1 positive status in 90 of 95 cases (94.7%). The concordance for PD-L1 status was lower when comparing SC1 vs SC2 (66.3%, 63/95 cases) or SC1 vs SC3 (71.5%. 68/95 cases). Regardless of the SC used, PD-L1 was not significantly associated with RFS.

Table 1			
Scoring criteria	**Negative**	**Low expressor**	**High Expressor**
SC1 (lung)	TC<1%	TC 1-49%	TC≥50%
SC2 (pembrulizumab)	TC and IC<1%	TC or IC≥1%	
SC3 (atezolizumab, avelumab)	IC<5%	IC 5-10%	IC>10%

Conclusions: There is no clinically validated standardized system for PD-L1 scoring in BC with regards to cutoffs and cellular components evaluated. In this limited cohort, SC2 and SC3 (used in ongoing CTL) were highly concordant and identified more patients than SC1 who might be considered for immunotherapy. A robust scoring recommendation for PD-L1 as a predictive marker in BC is needed; this should ideally be based on data from randomized CTL of immunotherapy.

1982 Deep Learning Can Distinguish Gleason Pattern 4 Cribriform Glands from Fused Small Glands in Prostate Cancer

John Bukowy[1], Sean McGarry[1], Allison Lowman[1], Peter Laviolette[2], Kenneth Iczkowski[1]
[1]Medical College of Wisconsin, Milwaukee, WI, [2]Milwaukee, WI

Disclosures: John Bukowy: None; Sean McGarry: None; Allison Lowman: None; Peter Laviolette: None; Kenneth Iczkowski: None

Background: Within Gleason 4 prostate cancer, larger, cribriform glands ($G4_{cg}$) are a recognized adverse prognostic finding (PMID:28820750) compared with the identically-graded fused small to poorly-formed glands ($G4_{fg}$). This study develops an algorithm for automated distinction and quantification of these subtypes.

Design: Twenty-eight patients undergoing radical prostatectomy were prospectively recruited for this study. Whole-mounted prostatectomy slides were digitized and patterns annotated by color-codes. A subset of individual tiles was then extracted from regions annotated, including $G4_{fg}$ and $G4_{cg}$. Using the convolutional neural network structure of Alex Krizhevsky et al. (Alexnet, Adv. in Neural Information Processing Systems, 1:1097-1105, proceedings 2012) a network was trained to perform binary classification of $G4_{fg}$ or $G4_{cg}$ when given a 227x227 RGB image of a G4 region. The training dataset constructed across 28 patients included foci of $G4_{fg}$ from 23 patients, and $G4_{cg}$ from 14 patients, yielding 654 $G4_{fg}$and 301 $G4_{cg}$ sample tiles. Training was performed using a 10x repeated random sub-sampling validation with a 70/30 training/validation split. Receiver operating characteristic (ROC) curves were generated for each trained model. As a qualitative analysis of what features the algorithm used to resolve each class, a deep-dream representation of each classifier was rendered and compared to sample images.

Results: Fig. 1 shows the result of the ROC analysis for 10 trained classifiers, where the area-under-the-curve (AUC) of the resulting ROC curve was 0.8962 ± 0.0041. **Fig. 2** shows the filtered, deep-dream representation of classifiers for $G4_{fg}$ (**a**) and $G4_{cg}$ (**b**). Puncta are further apart in $G4_{fg}$ while $G4_{cg}$ has many puncta close together with periodic intervening openings. These are compared to representative samples of a histology tile given to the algorithm for training purposes (**c**, $G4_{fg}$ and **d**, $G4_{cg}$).

Figure 1 - 1982

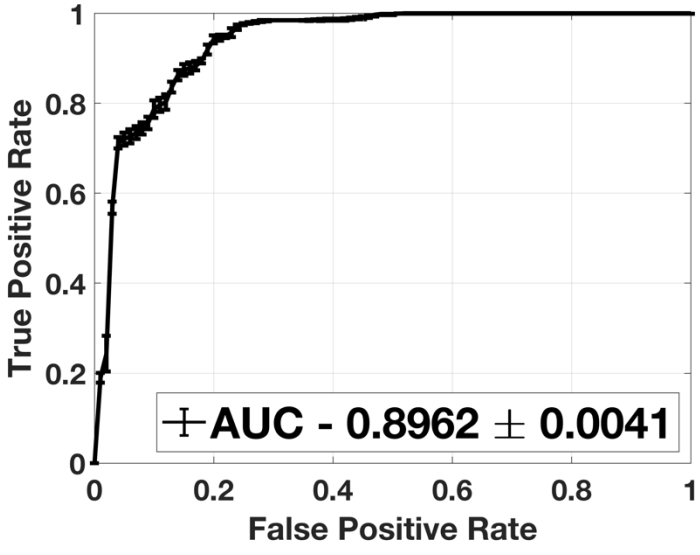

Figure 2 - 1982

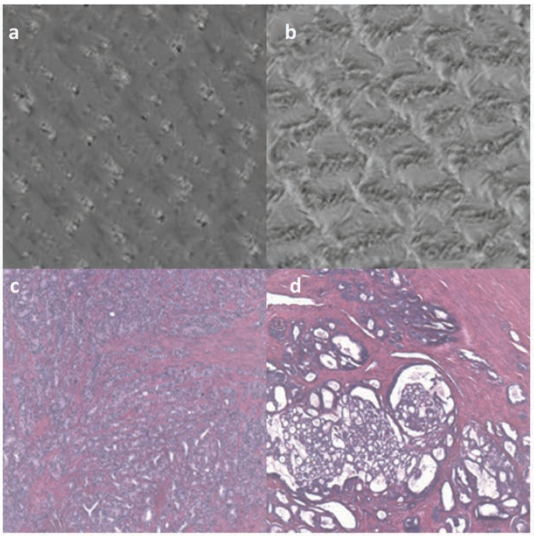

Conclusions: We present a highly accurate automated algorithm to distinguish $G4_{fg}$ left and $G4_{cg}$. Direct applications of this method include pipeline integration to further sub-classify identified Gleason 4 regions as a prognostic workflow. Future applications may expand its use in a multi-step classifier to reduce grading error when discriminating problematic Gleason patterns, such as grade 3 versus 4.

1983 Nonlinear Microscopy: Rapid Imaging of Freshly Excised Tissue, Methodology and Instrumentation

Lucas Cahill[1], Seymour Rosen[2], Tadayuki Yoshitake[3], Michael Giacomelli[4], Yubo Wu[2], Liza Quintana[2], Jared Ahrendsen[2], Yaileen D Guzman-Arocho[2], Beverly Faulkner-Jones[5], James Connolly[6], James G. Fujimoto[3]
[1]MIT-Harvard, Cambridge, MA, [2]Beth Israel Deaconess Medical Center, Boston, MA, [3]Massachusetts Institute of Technology, Cambridge, MA, [4]Massachusetts Institute of Technology, Rochester, NY, [5]Boston, MA, [6]Beth Israel Deaconess Medical Center, Jamaica Plain, MA

Disclosures: Lucas Cahill: None; Seymour Rosen: None; Tadayuki Yoshitake: None; Michael Giacomelli: None; Yubo Wu: None; Liza Quintana: None; Jared Ahrendsen: None; Yaileen D Guzman-Arocho: None; Beverly Faulkner-Jones: None; James Connolly: None; James G. Fujimoto: None

Background: Nonlinear microscopy (NLM) is a versatile imaging technique that enables visualization of tissue similar to conventional optical microscopy. However, NLM can image freshly excised, intact tissue and, unlike frozen section analysis, NLM does not require freezing, physical sectioning, or slides. Thus, all tissue imaged via NLM can be subsequently processed for standard histopathology without impairment. Manipulation of the z axis (focus into the tissue) enables tissue examination of depths up to ~100 µm into the tissue analogous to serial sectioning.

Design: Various tissues were stained with fluorescent nuclear (acridine orange) and stromal/cytoplasmic (sulforhodamine) dyes for 1 to 2 minutes and rinsed in saline for 10 seconds. The specimens were placed on a holder with a glass surface then onto an NLM microscope (Fig. 1). The specimen holder was constructed to hold large intact specimens (up to 10x8 cm) and small fragments of tissue such as core needle biopsies. Additionally, saline and formalin could be added during or after NLM imaging via ports on the holder's lid. Images were generated by nonlinear excitation of the fluorescent dyes, where signal is only generated at the focus of the objective, and displayed in a color scale similar to H&E.

The specimens were first evaluated in real-time at magnifications ranging from 5X to 20X analogous to a standard light microscope. Individual images were then mosaicked to assemble large montages analogous to the output of a slide scanner. Post imaging, specimens were submitted for H&E histology for comparison. Of note, breast and prostate tissue were submitted for molecular analysis.

Results: Normal tissues (adipose, skeletal muscle, and bone) and inflammatory and neoplastic processes in organs (skin, breast, prostate, kidney, lung) could be imaged (Fig. 2). Cytologic details including muscle striations and nucleoli were recognized and enhanced. Formalin fixation does not affect the imaging sequence and NLM imaging does not impair subsequent routine tissue processing, staining, immunohistochemistry, FISH or RNA/DNA analysis.

Figure 1 - 1983

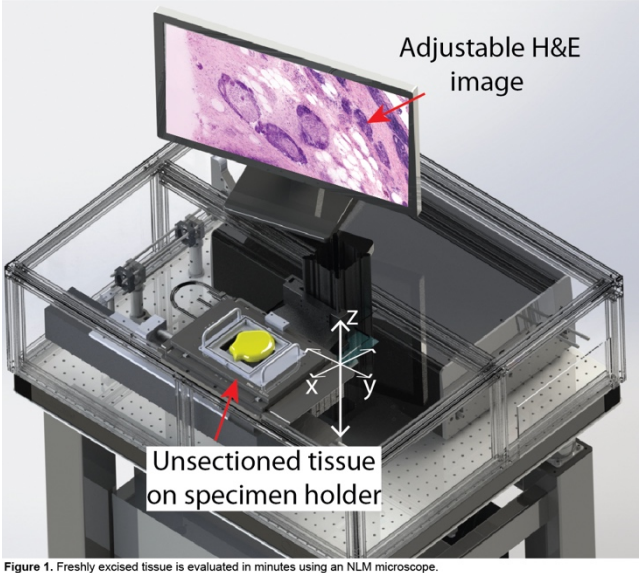

Figure 1. Freshly excised tissue is evaluated in minutes using an NLM microscope.

Figure 2 - 1983

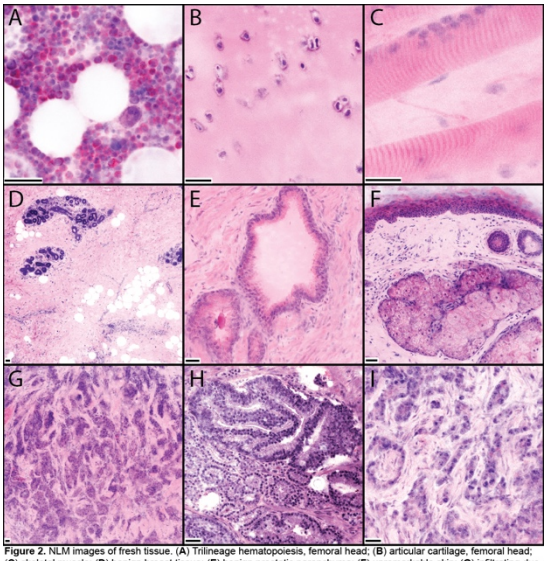

Figure 2. NLM images of fresh tissue. (**A**) Trilineage hematopoiesis, femoral head; (**B**) articular cartilage, femoral head; (**C**) skeletal muscle; (**D**) benign breast tissue; (**E**) benign prostatic parenchyma; (**F**) unremarkable skin; (**G**) infiltrating ductal carcinoma, breast; (**H**) prostatic adenocarcinoma, Gleason 4 pattern; (**I**) prostatic adenocarcinoma, Gleason 5 pattern.

Conclusions: NLM is a new and rapid tissue evaluation technique with great potential for intraoperative and intraprocedural tissue analysis.

1984 Point-of-Care Detection of KSHV and EBV to Diagnose Kaposi Sarcoma and Endemic Burkitt Lymphoma

Ethel Cesarman[1], Andrea Gardner[2], Ryan Snodgrass[3], Varun Lingaiah Kopparthy[3], Aggrey Semeere[4], Priscilla Namaganda[4], Robert Lukande[5], Miriam Laker-Oketta[4], Esther Freeman[6], Megan Wenger[7], Toby Maurer[7], Jeffrey Martin[7], David Erickson[3]
[1]Weill Cornell Medical College, New York, NY, [2]Weill Cornell Medical College, Austin, TX, [3]Cornell University, Ithaca, NY, [4]Makerere University, Kampala, Uganda, [5]Kampala, Uganda, [6]Massachusetts General Hospital, Harvard Medical School, Boston, MA, [7]University of California, San Francisco, San Francisco, CA

Disclosures: Ethel Cesarman: None; Andrea Gardner: None; Ryan Snodgrass: None; Varun Lingaiah Kopparthy: None; Robert Lukande: None; Esther Freeman: None; David Erickson: None

Background: Malignancies caused by KSHV/HHV-8 (Kaposi sarcoma, KS) and EBV (endemic Burkitt lymphoma, eBL) are most common in Sub-Saharan Africa where diagnosis is hampered by difficulty accessing pathology support and ancillary testing like immunohistochemistry (IHC). This leads to patients presenting with advanced disease resulting in poor clinical outcomes. While KS requires a biopsy, diagnosis of eBL can be achieved using fine needle aspiration (FNA) cytological specimens. We hypothesized that molecular testing of viral genomes at the point-of-care enhances and speeds the diagnosis of associated cancers.

Design: We developed a low-cost portable device, called TINY (Tiny Isothermal Nucleic Acid Amplification System). This lightweight device performs loop-mediated isothermal amplification (LAMP) and runs on a variety of power sources, including solar. We compared molecular detection of KSHV using qPCR and TINY, using H&E and IHC for LANA as the gold standard. Biopsies were taken and DNA extraction was performed, with a portion fixed in formalin. For EBV detection in eBL, we have developed a process-free cells-to-LAMP assay that seamlessly integrates into TINY based on a solution that allows extraction-free amplification. This method was tested with eBL cell lines and mouse xenografts that mimic material obtained by FNA.

Results: For KSHV detection in KS, qPCR had a sensitivity of 93% and specificity of 91% (N=347) and TINY had a specificity and sensitivity of 91% (N=128). Testing conducted in Uganda on actual KS biopsies provided results within 3 hours, and the longest time went to DNA extraction from skin biopsies. For EBV testing, we found that the cells-to-LAMP assay has a limit of detection of 90 copies per reaction with sensitivity of 99% at a threshold cutoff time of 30 minutes. Material obtained from a FNA of an eBL mouse xenograft detected EBV in both regular qPCR equipment and TINY (Figure).

Figure 1 - 1984

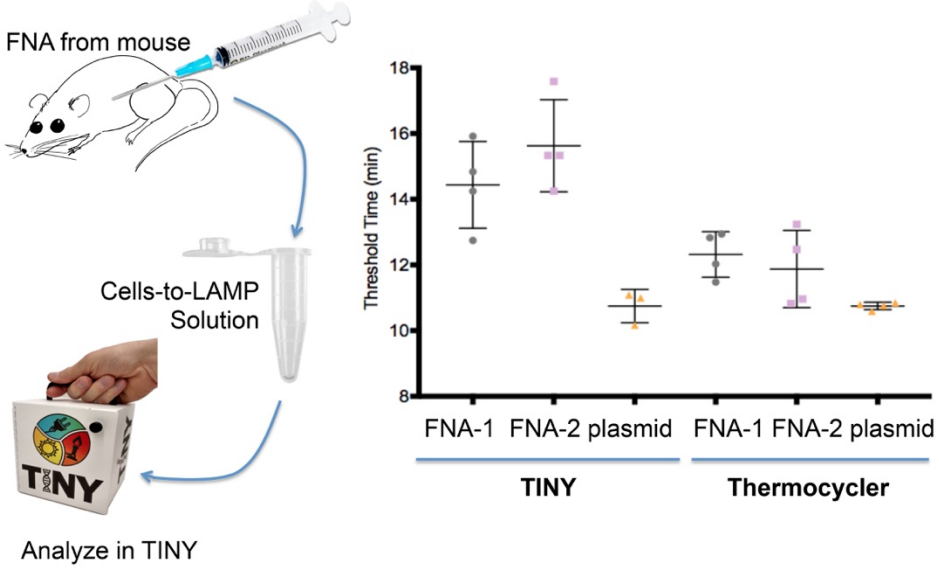

Conclusions: TINY allows for rapid diagnosis of KS at the point of care, with good specificity and sensitivity. However, DNA extraction is necessary from skin biopsies. A new cells-to-LAMP solution produces amplification threshold values on the same order as DNA purified with a commercial kit, and allows application of this method to cytology specimens, as tested for EBV in eBL, but potentially for others such as HPV. In combination with our established TINY system, a direct cells-to-LAMP system has been developed to rapidly detect EBV in lymphomas from FNA at the point-of-care.

1985 Cerium Compounds Effect on Post-Burn Scar Tissue Maturation in the In Vivo Experiment (Electron Microscopic Study)

Irina Chekmareva[1], Olga Legon'kova[1], Oxana Paklina[1], Alina Korotaeva[1], Sergey Ukhin[1], Pavel Sarygin[1], Dmitry Kalinin[1]
[1]A.V. Vishnevsky Institute of Surgery, Moscow, Russian Federation

Disclosures: Irina Chekmareva: None; Olga Legon'kova: None; Oxana Paklina: None; Alina Korotaeva: None; Sergey Ukhin: None; Pavel Sarygin: None; Dmitry Kalinin: None

Background: Transmission electron microscopy (TEM) is an objective research method that allows determinationof cerium compounds effect on post-burn scar tissue maturation on cellular level.

Design: Twenty five rats of *Vistar* breed were injured via IInd degree burn to the previously depilated hip area without epidermis damage. On the 26th day one of cerium preparations (0.5 ml) was subcutaneously injected into the formed scar area at intervals of 3 to 5 days. Totally, four injections of the drug were performed.The following drugs were studied in four groups of animals: Ist–0.05 % by weight nanodispersed cerium dioxide(NDC) solution; IInd–0.5% by weight NDC solution; IIIrd –0.05 % by weight cerium chloride (III) solution; IVth–0.5 % by weight cerium chloride (III) solution. Morphological examination (histological and electron microscopic) was performed on the 29th and 42rd days after the burn injury.

Results: On the 29th day after the injection of cerium preparations only in the IVth group of animals cerium accumulations in the macrophages' cytoplasm, endotheliocytes, fibroblasts were noted (Fig. a), viability and functional activity of the cells were retained. In connective tissue samples of the other animal groups cerium was not found. On the 42nd day intracellular clusters of cerium in scar tissue cells of the all experimental animal groups were found, as in vacuoles (Fig. b) and freely in the cytoplasm, which did not lead to intracellular destructive processes. The wound defects were filled with scar tissue. Collagen fibers were oriented mainly parallel to the surface of the epidermis. Mature cells with moderate or weak functional activity in the population of fibroblasts were dominated.

Figure 1 - 1985

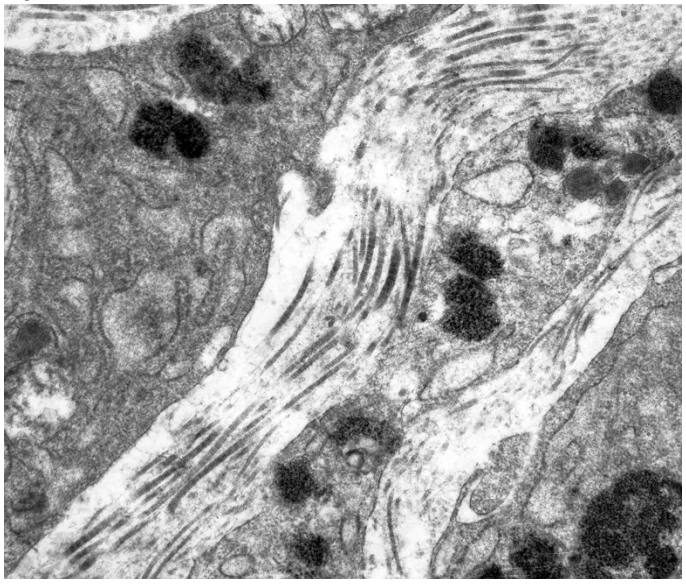

Figure 2 - 1985

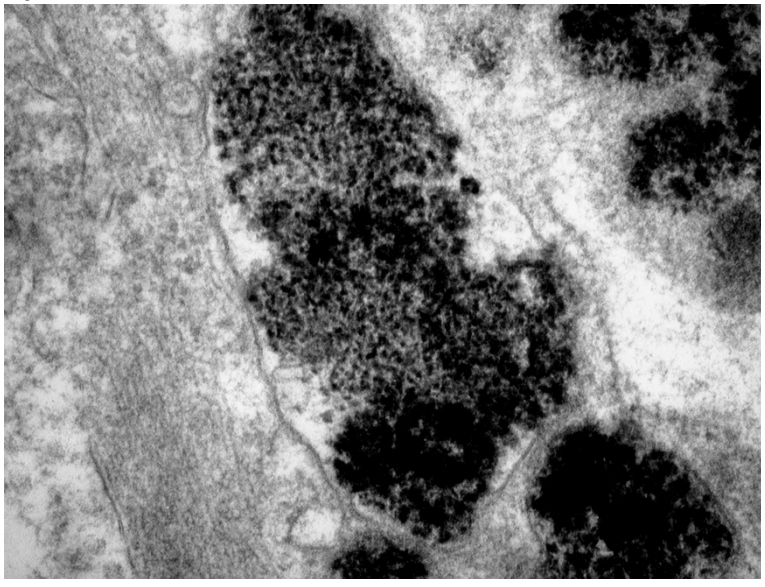

Conclusions: Cerium compounds, as in ionic and nanoparticulate forms, does not lead to destructive intracellular processes, indicating the absence of cytotoxicity. Intracellular clusters of cerium of different sizes – from single to multiple, do not lead to functional activity decreasing of fibroblasts, macrophages, endotheliocytes.

1986 Automatic Bone Marrow Cell Classification on Digital Images by an Artificial Intelligence (AI)-Based System: a Pilot Study

Mingyi Chen[1], Xiang Xu[2], James zhang[3], Xianggui Peng[4], Gusheng Tang[5], Fang Fengqi[6], Ju Lu[7], Jianyu Rao[8]
[1]University of Texas Southwestern Medical Center, Dallas, TX, [2]UT Southwestern Medical Center, Southlake, TX, [3]Sir Run Run Shaw Hospital, Hangzhou, China, [4]Xinqiao Hospital, Chongqing, China, [5]Changhai Hospital, Shanghai, China, [6]The First Hospital Dalan Medical University, Dalian, China, [7]Zhiwei Information Technology Co., Ltd., Hangzhou, China, [8]Los Angeles, CA

Disclosures: Mingyi Chen: *Advisory Board Member*, Zhiwei Tech; Xiang Xu: None; James zhang: None; Xianggui Peng: None; Gusheng Tang: None; Fang Fengqi: None; Ju Lu: None; Jianyu Rao: None

Background: The nucleated-cell differential counts on the bone marrow aspirates is requisite for the clinical diagnosis of hematological malignancy. Manual bone marrow differential count is time consuming, tedious, and lack of consistency. In this pilot study, we applied an AI-based automatic system to perform differential cell count of whole slide scanned bone marrow aspirates to determine the feasibility.

Design: We randomly scanned bone marrow aspirates of patients from multiple medical centers with a spectrum of diagnosis using a digital microscopy system at a magnification of ×400. An AI-based system was designed to select the areas of marrow spicules and recognize specific morphological features as criteria to classify the cell types. Two experienced pathologists independently reviewed the digital imagines of the cells to confirm the cell types.

Results: In our initial test sets of 1500 cases, we achieved a promising classification performance with average accuracy value of 97.0% for erythroid serires, 96.0% for granulocytic series, 81.2% for monocytic series, 94.6% for lymphocytic series, and 94.2% for plasma cell series. The differential cell percentage of the automated count based on 500 cell counts correlated to differential cell percentage provided by the pathologists with the correlation coefficient at 0.95 ($P < 0.01$). The overall sensitivity and specificity of the system are found to be 84.4% and 97.9%, respectively. The AI-based learning accuracy appears also correlated with the number of cells analyzed in each category, whereas over 30,000 cells will be needed to reach 90% and above accuracy. Our preliminary data based on 5,000 cells achieves the accuracy value of immature cells/blasts are approximately 84.0%. The technical challenge remains in the distinguishing the early erythroblasts from myeloblasts and atypical promyelocyes or promonocytes (the blasts equivalents). Therefore, the system needs more training in order to recognize the subtle difference in nuclear and cytoplasmic features.

Cell types	Sensitivity	Specificity	Accuracy
Immature cells/Blasts	69.9%	98.1%	84.0%
Erythroid series	95.5%	98.5%	97.0%
Granulocytic series	95.8%	96.2%	96.0%
Monocytic series	63.8%	98.6%	81.2%
Lymphocytic series	92.8%	96.3%	94.6%
Plasma cell series	88.7%	99.7%	94.2%

Conclusions: Based on our initial training set analysis, our well designed AI-based imagine recognition system is a reliable tool for bone marrow smear differential analysis. The large scale multi-center validation studies are warranted to further confirm the clinical utility of the system.

1987 Multi-Center Assessment of Reproducibility of Mass Spectrometry Imaging

Soeren-Oliver Deininger[1], Christine Bollwein[2], Rita Casadonte[3], Petra Wandernoth[3], Rémi Longuespée[4], Katharina Kriegsmann[5], Mark Kriegsmann[5], Joerg Kriegsmann[6], Wilko Weichert[7], Peter Schirmacher[4], Alice Ly[1], Kristina Schwamborn[8]
[1]Bruker Daltonik GmbH, Bremen, Germany, [2]Institute of Pathology, Technical University Munich, Munich, Germany, [3]Proteopath GmbH, Trier, Germany, [4]Institute of Pathology, Heidelberg University Hospital, Heidelberg, Germany, [5]University Hospital Heidelberg, Heidelberg, Germany, [6]MVZ für Histologie, Zytologie und Molekulare Diagnostik, Trier, Germany, [7]Muenchen, Germany, [8]Munich, Germany

Disclosures: Soeren-Oliver Deininger: None; Christine Bollwein: None; Rita Casadonte: None; Petra Wandernoth: None; Rémi Longuespée: None; Katharina Kriegsmann: None; Mark Kriegsmann: None; Joerg Kriegsmann: None; Wilko Weichert: *Speaker*, Lilly, BMS, MSD, Novartis, Roche, AstraZeneca; *Advisory Board Member*, BMS, MSD, Novartis, Pfizer, Roche, AstraZeneca, Boehringer, Merck; *Grant or Research Support*, Roche, BMS, MSD, Bruker; Peter Schirmacher: *Grant or Research Support*, Bruker; Alice Ly: None; Kristina Schwamborn: *Speaker*, Roche, MSD, BMS

Background: Classification of tissues based on label-free mass spectrometric phenotypes measured directly from sections is a promising tool for clinical research. However, reproducibly measuring mass spectra can be challenging and comprehensive studies assessing the variation across different sites are largely lacking. In this work we have compared the reproducibility of Matrix-Assisted-Laser-Desorption/Ionization MALDI mass spectrometric imaging (MALDI-MSI) based tissue classifications measured at three different sites.

Design: A tissue microarray (TMA) was constructed to contain human formalin-fixed paraffin-embedded (FFPE) samples representing different tumors. The tumors were leiomyoma, seminoma, mantle cell lymphoma, melanoma, invasive ductal carcinoma of the breast and squamous cell carcinoma of the lung. Each tumor type was sampled from 5 different subjects at each three different sites. These samples were prepared for MALDI-MSI and measured at three different sites using a standard protocol. A linear discriminant analysis (LDA) was used to generate a classifier for these 6 tumor types and all pairwise classifications. The accuracy of the LDA models was evaluated by a two-step "leave-one-core-out-leave-one-measurement-out" cross-validation so that the classifier has never seen the individual subject nor the measurement. Unsupervised clustering and principal component analysis (PCA) were used to assess overall spectral similarities.

Results: The accuracy of the classification on the individual pixel level was 76% for the 6-class classifier and up to 93% for the pairwise classifications. We did not see a systematic influence of the sampling site or the measurement site on the classification accuracy.

Unsupervised clustering and PCA analysis of mass spectral similarities also indicated that the biological difference between tissue states showed a larger influence on the spectral phenotypes than sampling site or measurement site.

Conclusions: To our knowledge this is the first study that has evaluated the site-to-site reproducibility of MALDI-MSI classification from FFPE tissue using clinical samples. Our initial results indicate that MALDI-MSI can be performed at a level that allows relevant multi-center research studies.

1988 Myxoinflammatory Fibroblastic Sarcoma: Ultrastructural Study of 7 Cases

Hugo Dominguez-Malagon[1], Guillermo Corredor[2], Claudia Haydee Caro[3]
[1]Instituto Nacional de Cancerología, Naucalpan, EM, Mexico, [2]Instituto Nacional de Cancerología, Mexico City, DF, Mexico, [3]Instituto Nacional de Cancerologia, Mexico City, DF, Mexico

Disclosures: Hugo Dominguez-Malagon: None

Background: Mixoinflammatory fibroblastic sarcoma is a locally aggressive neoplasm with a distinctive morphology. Composed by fusiform and epithelioid fibrocellular areas, and myxoid areas in "dilapidated brick wall" with variable quantity of three cell types: Reed-Stemberg like cells, pseudolipoblasts and cells with emperipolesis. To date, just over 400 cases have been described; 23 high-grade and 7 with atypical characteristics have been described. It is presented in a wide age range with an average of 40 years, and 66 years high-grade variants; it has a local recurrence between 22 and 67% with metastatic potential of 2 to 38%. No distinctive immunohistochemical profile, with variable expression of D2-40, CD34, CD68, Cyclin D1, CD163, C-kit and EGFR.

Design: Seven cases confirmed by clinical and morphological features with usual profile of immunohistochemistry were chosen from the biopsies received in the pathology service of the Instituto Nacional de Cancerología. Paraffin embed Block and

Results: Of the 7 cases selected, 4 of women and 3 of men, with an age range between 21 and 79 years (mean of 57 cm and median of 55 cm). Three cases were distal, three proximal and one in head; measurements between 1.5 and 15 cm (mean of 5.9 cm and median of 4.5 cm). The immunohistochemical profile, all cases were positive for CD68, 5 cases were positive for D2-40, CD163 and Cyclin-D1 respectively. Only 2 cases were positive to C-kit and one case to EGFR. Ultrastructurally, all the lesions showed irregular nuclei with macronucleoli, binucleation, abundant rough endoplasmic reticulum with dilated cisterns. Five cases with abundant lysosomes and phagolysosomes; Four cases showed nuclear indentation due to the dilatation of the cisterns (cells in "soccer ball") and abundant intermediate filaments. Three cases with multinucleation and a single case with osteoclastic giant cells and histiocytes in the dedifferentiated portion.

ID	SEX	AGE	STATUS	METS	LOCATION	SIZE	DX	MACRONUCLEOLI	IRREGULAR NUCLEI	RER ABUNDANT	DILATED CISTERNAE	SOCCER BALL	PHAGOLYSOSOME-LYSOSOME	INT. FILAMENT	BINUCLEATED	MULTINUCLEATED	OSTEOCLAST	D2-40	CD68	CD163	CYCLIN-D1	C-KIT	EGFR
ME5602	F	55	ALIVE	NO	LEFT HAND	2	MIFS ACRAL	YES	YES	YES	YES	NO	YES	YES	YES	NO	NO	POSITIVE	POSITIVE	POSITIVE	NEGATIVE	NEGATIVE	NEGATIVE
ME5687	M	54	ALIVE	NO	RIGHT KNEE	15	MIFS	YES	YES	YES	YES	YES	YES	NO	YES	NO	NO	POSITIVE	POSITIVE	POSITIVE	POSITIVE	NEGATIVE	NEGATIVE
ME6301	F	79	ALIVE	LUNG	RIGHT SHIN	4.5	MIFS HIGH GRADE	YES	YES	YES	YES	NO	NO	NO	YES	YES	NO	POSITIVE	POSITIVE	NEGATIVE	POSITIVE	NEGATIVE	NEGATIVE
ME6341	M	67	ALIVE	LUNG	RIGHT FOREARM	8.5	MIFS DEDIFFERENTIATED	YES	YES	YES	YES	YES	YES	NO	YES	NO	YES	POSITIVE	POSITIVE	POSITIVE	POSITIVE	NEGATIVE	NEGATIVE
ME6345	F	68	ALIVE	NO	RIGHT ARM	8	MIFS ABUNDANT INFLAMATION	YES	YES	YES	YES	NO	NO	YES	YES	NO	NO	POSITIVE	POSITIVE	NEGATIVE	POSITIVE	NEGATIVE	NEGATIVE
ME6346	F	55	ALIVE	NO	FINGER LEFT HAND	1.5	MIFS ACRAL	YES	YES	YES	YES	YES	YES	YES	YES	YES	NO	NEGATIVE	POSITIVE	POSITIVE	NEGATIVE	POSITIVE	NEGATIVE
ME6753	M	21	ALIVE	NO	CHEEK	2	MIFS	YES	YES	YES	YES	YES	YES	YES	YES	YES	NO	NEGATIVE	POSITIVE	POSITIVE	POSITIVE	POSITIVE	POSITIVE

Figure 1 - 1988

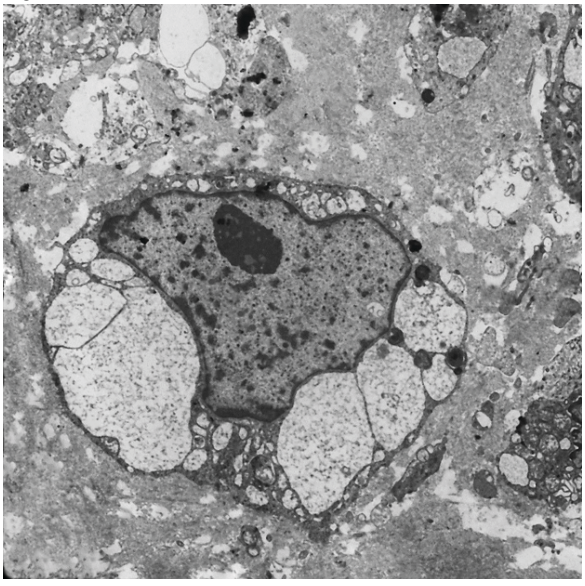

Figure 2 - 1988

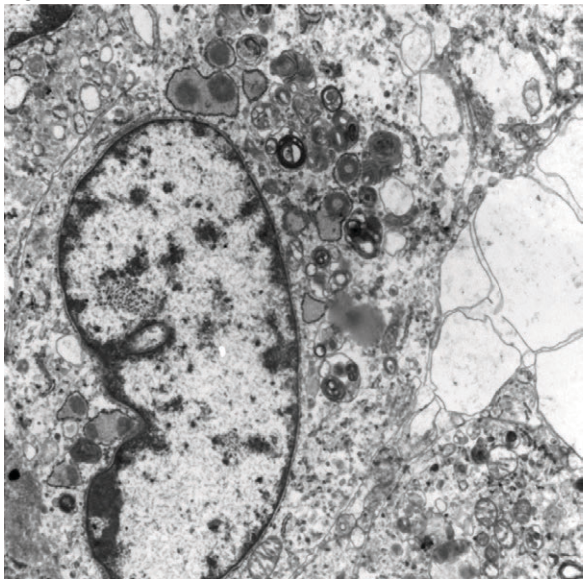

Conclusions: Despite being an entity studied in terms of its histomorphology and its molecular profile, there are no published studies that accurately report the distinctive ultrastructural features. We can say that only the myxoinflammatory fibroblastic sarcoma so far evidence modified fibroblastic phenotype and variable proportion of macrophage differentiation.

1989 The Impact of Pre-analytical Parameters on PD-L1 Immunohistochemistry: Concordance across Four Tissue Processing Protocols using Two PD-L1 Clones in Multiple Tumor Types

Michelle Downes[1], Bin Xu[2], Samira Alminawi[1], Patrice Boulianne[1], Yan Ming Shang[1], Elzbieta Slodkowska[3]
[1]Sunnybrook Health Sciences Centre, Toronto, ON, [2]Sunnybrook Health Sciences Centre - University of Toronto, New York, NY, [3]Sunnybrook Health Sciences Centre - University of Toronto, Toronto, ON

Disclosures: Michelle Downes: None; Bin Xu: None; Samira Alminawi: None; Patrice Boulianne: None; Yan Ming Shang: None; Elzbieta Slodkowska: None

Background: The evolution in immuno-oncology has placed PD-L1 tissue interpretation under scrutiny. Multiple clones exist and the impact of various pre-analytical factors on tissue expression has been underexplored. We assessed two commonly available clones (SP263 and 22C3) across a variety of malignancies using four separate tissue processing protocols and two separate tissue processors to determine the effect on (1) percentage positive cases and (2) raw percentage tumour cells (TC).

Design: Formalin fixed tissue of 109 tumors was collected and processed on two tissue processors using four separate protocols: Pathos delta (P1 - rapid for biopsies, P2 - routine, P3 - for fat rich tissue), and Leica ASP330S for fat rich tissue (P4). Triplicate core (1mm) tissue microarrays were created following processing and included: colorectal carcinomas, n=28, breast carcinomas, n=22, renal tumors, n=21, head/neck squamous cell carcinomas, n=13, melanomas, n=11, bladder urothelial carcinomas (UC), n=11, endometrial carcinoma, n=1, Merkel cell carcinoma, n=1 and papillary thyroid carcinoma, n=1. Sequential sections from each block were stained with PD-L1 clones SP263 and 22C3 on Benchmark and Omnis platforms, respectively. The percentage TC for each case was averaged across three cores. Cases were designated as positive/negative using the companion algorithm for the antibody (bladder algorithm for UC, lung algorithm for all other tumors). Fleiss' kappa (k) analysis and intraclass correlation coefficients (ICC) were calculated.

Results: The concordance across all four protocols for tumor designation as PD-L1 positive/negative was k =0.531 for SP263 and k= 0.503 for 22C3. K values were higher when assessing cut offs <1% and >50% (k= 0.660-0.720) compared with 1-5%, 5-25%, 25-49% cut-offs (k=0.089-0.412). Protocol P3 had the lowest concordance between the clones, k=0.459, with P2 having the highest, k=0.730. The overall ICC for TC% was 0.726 and 0.692 for 22C3 and SP263, respectively. The P2 protocol had the highest ICC between the clones, 0.916 vs 0.828 (lowest) for P3.

Figure 1 - 1989

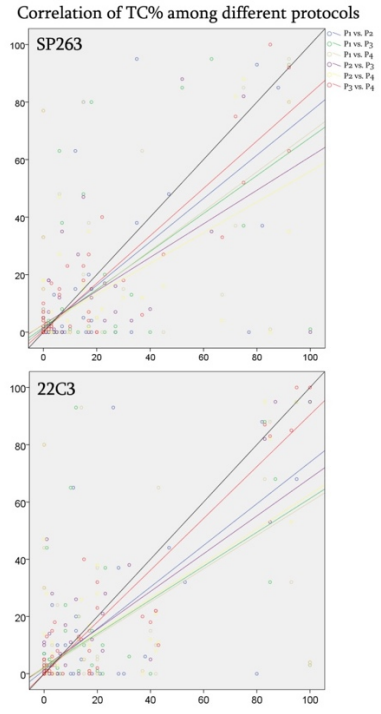

Conclusions: The choice of tissue processing protocol impacts staining of TC and designation as PD-L1 positive/negative regardless of antibody clone. Optimization and validation of pre-analytic processes are critical for correct PD-L1 biomarker interpretation.

1990 A Chromogenic In Situ Hybridization (CISH) Technique for Assessing Telomeric DNA Length in Formalin-Fixed Tissue Sections

Onur Ertunc[1], Qizhi Zheng[1], Erica Smearman[2], Jessica Hicks[3], Jacqueline Brosnan-Cashman[1], Tracy Jones[3], Levent Trabzonlu[1], Christopher Heaphy[3], Alan Meeker[3], Angelo De Marzo[1]
[1]Johns Hopkins University, Baltimore, MD, [2]Emory University, Atlanta, GA, [3]Johns Hopkins University School of Medicine, Baltimore, MD

Disclosures: Onur Ertunc: None; Erica Smearman: None; Jessica Hicks: None; Jacqueline Brosnan-Cashman: None; Tracy Jones: None; Levent Trabzonlu: None; Christopher Heaphy: None

Background: Telomere dysfunction has been implicated in cancer and other age-related diseases. Thus fluorescent in situ hybridization methods have been developed to evaluate telomeres directly in cells and tissues. However, fluorescent based tissue assays are cumbersome for pathologists/investigators, both in clinical and research settings. Recently, we and others have employed Advanced Cellular Diagnostics (ACD) RNAscope technology for the use in DNA *in situ*hybridization (PMIDs: 28034905, 29462571). Here we present a robust chromogenic technique for telomere-specific *in situ* hybridization (CISH) developed for use with archival formalin-fixed paraffin embedded tissue samples based on ACD RNAscope.

Design: *In situ* hybridization was performed on simulated tissue using isogenic cell lines programmed to have differing telomere lengths that were subjected to formalin fixation and paraffin embedding (FFPE). Further, clinical FFPE tissues of prostate cancer and precursor lesions, which are known to harbor short telomeres in the vast majority of cases, were used.

Results: Telomeric signals using the chromogenic assay showed a continuum of increased intensity and extent in cell lines with increasing telomere lengths, and the nuclear area fraction (Halo, Indica labs) correlated well with the known quantitative fluorescent based assay (r^2 = 0.86, p = 0.0025, linear regression). (**Figure 1)** Using an FFPE tissue microarray of prostate cancer and matched normal, there were strong telomeric signals in the normal epithelium and stromal cells, with marked reductions clearly visible in most tumor cells. Using frozen sections from 21 patients from 68 tissue blocks, there was marked reduction in telomere signals in 41 of 41 cancer lesions and 44 of 44 high grade PIN lesions. In invasive carcinoma lesions, 16/41 (39%) showed telomere length heterogeneity, while none of the PIN regions and 4 of 7 (57%) regions of intraductal carcinoma showed telomere length heterogeneity that would have been very difficult to pick up using the fluorescence-based assay. Finally, we combined telomere CISH with IHC for PIN4 and CK903 in a multiplexing. (**Figure 2)**

Figure 1 - 1990

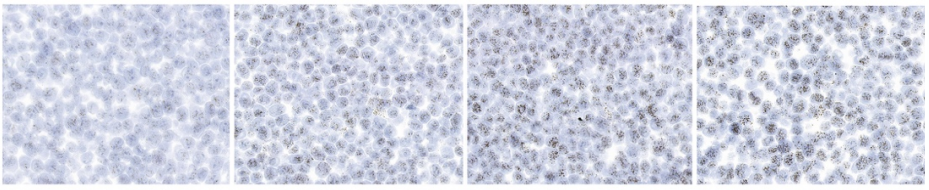

Figure 1. Telomere CISH in isogenic cell lines with increasing telomere length (from left with shortest, to right with longest telomeres).

Figure 2 - 1990

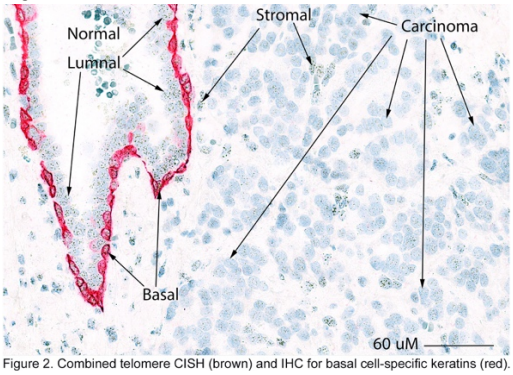

Figure 2. Combined telomere CISH (brown) and IHC for basal cell-specific keratins (red).

Conclusions: This new telomere CISH method is reproducible and quantitative and can be applied to FFPE sections. Since telomere shortening is common and often specific to neoplastic or preneplastic cells, and the assay can be combined with IHC, this approach should facilite studies on cancer precursors in many organ systems.

1991 Application of Nonlinear Microscopy in Dermatopathology: Identification of Basal Cell Carcinoma

Beverly Faulkner-Jones[1], Michael Giacomelli[2], James G. Fujimoto[3], Daihung Do[4]
[1]Boston, MA, [2]Massachusetts Institute of Technology, Rochester, NY, [3]Massachusetts Institute of Technology, Cambridge, MA, [4]Beth Israel Deaconess Medical Center, Boston, MA

Disclosures: Beverly Faulkner-Jones: None; Michael Giacomelli: None; James G. Fujimoto: None; Daihung Do: None

Background: Nonlinear microscopy (NLM) is a versatile laser-based imaging technique that enables visualization of tissue in a similar manner to conventional optical microscopy. However, NLM can be used to image intact freshly excised tissue as well as formalin-fixed non-processed tissues without needing physical sectioning. NLM imaging is non-destructive, does not interfere with subsequent diagnostic tests, and enables detailed three-dimensional analysis of tissue specimens at video rate.

Design: Retrospective single-center study using discarded Mohs frozen tissue blocks for basal cell carcinoma. Frozen section slides (stained with H&E) were obtained from the Mohs case or an additional frozen section slide was cut from the block and then scanned. NLM was then used to examine these discarded frozen Mohs tissue blocks after thawing.

Results: Mohs sections were evaluated by frozen section in conjunction with subsequent NLM examination of thawed and flattened tissue blocks. Thawing did not appreciably alter the tissue appearance as compared to fresh tissue. Basal cell carcinoma could be identified and tumor-typed and the margins assessed (Figure 1). Left panel shows a nodular basal cell carcinoma. The right panel is a higher zoom view showing peripheral palisading and peritumoral mucin. Advantages of NLM over frozen section included being able to image intact subcutaneous adipose tissue without the fragmentation often seen in frozen sections. In addition, multiple tissue levels could be rapidly assessed.

Figure 1 - 1991

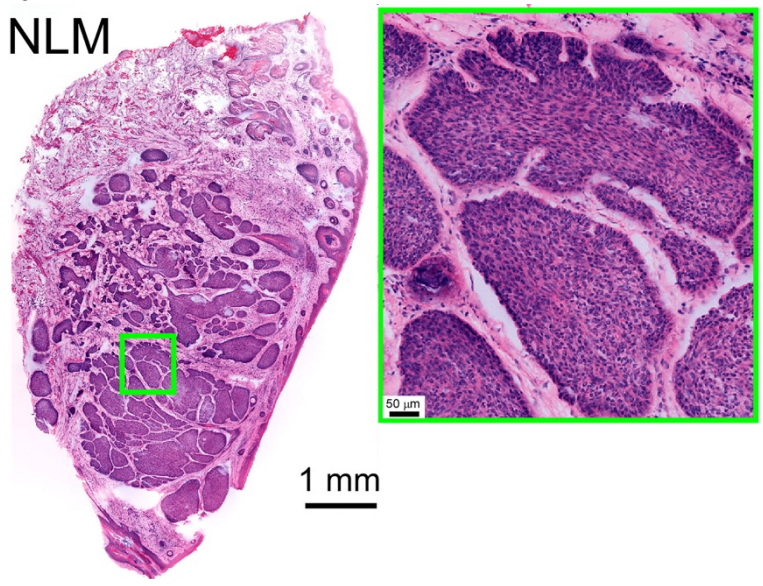

Conclusions: Nonlinear microscopy may be a useful in detecting basal cell carcinoma in Mohs surgery, possibly replacing frozen sections.

1992 Mosaic Expression of Over 2,000 Proteins Indicate Wide Diversity between Fast and Slow-Twitch Skeletal Muscle Fibers

Katherine Fomchenko[1], Marc Halushka[2]
[1]The Johns Hopkins University School of Medicine, Baltimore, MD, [2]Johns Hopkins University School of Medicine, Baltimore, MD

Disclosures: Katherine Fomchenko: None; Marc Halushka: None

Background: Skeletal muscle fiber types have different phenotypes (fast and slow twitch) based on the differential expression of many proteins, only some of which are known. We utilized a recently developed proteomic technique, HPASubC on the immunohistochemistry-stained Human Protein Atlas (HPA) tissue images to investigate variable protein expression of skeletal muscle.

Design: Utilizing HPASubC, 50,351 skeletal muscle images from HPA were obtained and assigned a score based on the level of confidence that the image displayed mosaicism in protein expression. These scores were used to characterize the proteins reflected in each image into confidence categories of “real,” “likely,” and “unknown” reflecting the strength of mosaicism. Stratified by this characterization, the proteins discovered were analyzed using Gene Ontology (GO) and String webtools, as well as comparisons to previously published skeletal muscle proteomic databases with mass-spectrometry based methods.

Results: In total, 2,143 proteins were differentially expressed in skeletal muscle, with 367 proteins in the “real,” 1,223 in “likely,” and 553 in “unknown” categories respectively. A significant number or our proteins were newly described with only 745 proteins (34.3%) and 578 proteins (27.0%) overlapping the mass-spectrometry based Human Skeletal Muscle Proteome and single fiber proteome work of the Mann laboratory[1]. Some of the novel “real” mosaic proteins identified from HPA data include GLRX2, TMEM161A, CLDND1, CCDC80, and SYDE1. The GO terms with the highest enrichment across all mosaic proteins were “fructose 1,6-bisphosphate metabolic process” and “muscle filament sliding,” while the “real” confidence category had the highest enrichment for “transition between fast and slow fiber” and “muscle filament sliding.”

Conclusions: Overall, our careful evaluation of >50,000 images using the technique of HPASubC yielded a number of proteins mosaic in skeletal muscle that had not been previously described. Many of these proteins had interesting functional classifications. This data will help us further understand the role of skeletal muscle in disease and aging.

(1) Murgia, M.; et al. Single Muscle Fiber Proteomics Reveals Fiber-Type-Specific Features of Human Muscle Aging. *Cell Rep.* **2017**, *19* (11), 2396–2409.

1993 Diagnostic Utility of Raman Spectroscopy in Differentiating Thyroid Nodules and Identifying Thyroid Cancer

Eric Huang[1], Marcos Soares de Oliveira[2], Michael Campbell[2], James Chan[2]
[1]University of Washington, Seattle, WA, [2]University of California, Davis, Sacramento, CA

Disclosures: Eric Huang: None; Marcos Soares de Oliveira: None; Michael Campbell: None; James Chan: None

Background: Fine-needle aspiration (FNA) is the cornerstone for evaluating most thyroid nodules. Unfortunately, approximately 15-30% of FNAs are considered “indeterminate”. Although the majority of these “indeterminate” nodules are ultimately benign, a thyroidectomy is required to rule out cancer, leading to unnecessary surgeries. In recent years, there has been a growing interest in using optical diagnostic techniques for cancer applications. Raman spectroscopy (RS) is a powerful optical technique for label-free chemical analysis that has been increasingly used in biomedical applications. Over the last decade, innovative techniques have advanced RS for optical biopsy due to its molecular fingerprinting characteristics. For example, recent studies using cryosectioned thyroid tissue have suggested that RS can potentially be used as a clinical tool for thyroid cancer diagnosis.

Design: A line-scan Raman microscope to obtain faster Raman molecular fingerprints of individual cells is performed. With IRB approved protocol, various thyroid nodules were obtained from the UC Davis biorepository. Individual follicular cells were isolated from tissues and prepared on microscope coverslips for Raman analysis.

Results: We used Raman imaging in combination with multivariate statistical analysis of the spectral data for objective identification and classification of single follicular cells from different types of human thyroid nodules. Individual cells were line-scanned while Raman spectra were simultaneously collected. We used post-processing algorithm to reconstruct the Raman map. Figure 1(a) shows a brightfield image of a single follicular cell. Figures 1(b) and 1(c) show the Raman map and the average Raman spectrum over the cell, respectively. Principal component analysis was also performed on the spectral data for objective differentiation of follicular cells. As shown in Figures 2(a) and 2(b), two different cancer and benign cell types, respectively, were clearly differentiated.

Figure 1 - 1993

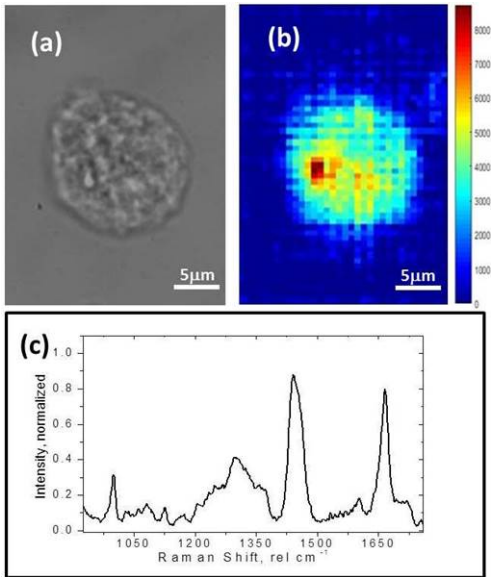

Figure 2 - 1993

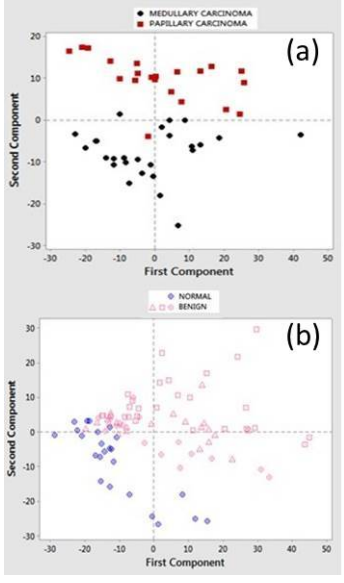

Conclusions: Our preliminary results indicate a high sensitivity and specificity for identifying different follicular cell types. So far, this technique has demonstrated to be a potential alternative for rapid and accurate improvement in thyroid nodule evaluation.

1994 Tissue Clearing Technology Allows Three-Dimensional Assessment of Pancreatic Tumor Tissue Obtained by Endoscopic Ultrasound-Guided Fine Needle Aspiration Biopsy (EUS-FNAB)

Eriko Ikeda[1], Jun Ushio[1], Yuki Kawasaki[1], Kensuke Yokoyama[1], Hironori Yamamoto[1], Hiroshi Onodera[2], Noriyoshi Fukushima[1]
[1]Jichi Medical University, Shimotsuke, Japan, [2]The University of Tokyo, Bunkyo, Japan

Disclosures: Eriko Ikeda: None; Jun Ushio: None; Yuki Kawasaki: None; Kensuke Yokoyama: None; Hironori Yamamoto: None; Hiroshi Onodera: None; Noriyoshi Fukushima: None

Background: For proper diagnosis and treatment selection for patients with pancreatic neoplasia, there is a growing need for subtyping and grading on small endoscopic ultrasound-guided fine needle aspiration biopsy (EUS-FNAB) specimens. However, those are limited compared with surgically resected specimens due to their small amount of cells. A goal of our research is to develop a protocol for the three-dimensional (3D) immunohistochemical evaluation using a lab-on-a-chip device with tissue clearing technology. In this present study, we evaluated the utility of the 3D counting of tumor cells and Ki-67 positive cells on EUS-FNAB specimens during the process of conventional histopathological assessment.

Design: Twelve FNAB tissue samples obtained from pancreatic neuroendocrine neoplasms, gastrointestinal stromal tumor and pancreatic ductal adenocarcinoma were applied. Fresh biopsy specimens were fixed quickly by formalin. After fixation, specimens were fluorescently stained with DAPI (4',6-diamidino-2-phenylindole) and Ki-67 antibody, and then optically cleared using transparency-enhancing technology: illumination of Cleared organs to Identify target molecules method (LUCID; Onodera H, 2014, Google Patents), and visualized using confocal laser microscopy. After obtaining the 3D images, all specimens were embedded with paraffin and were subsequently sectioned into thin slices and histopathologically assessed using hematoxylin–eosin (H&E) staining and Ki-67 immunostaining.

Results: All specimens were successfully cleared by LUCID and stained by DAPI in less than 30 mins. The 3D imaging with laser scanning microscopy enabled observation of adequate tumor cells that lost in conventional 2D assessments. Structural observation of the tumor tissue was also facilitated. Furthermore, the morphology of the samples after being cleared by LUCID was well preserved, and the quality of staining after 3D analysis was sufficient for conventional histopathological examination.

Conclusions: The tissue clearing and 3D image-analysis allowed us to obtain more precise tumor cell counting such as Ki-67 positive cells on FNAB specimens. The present first trial will lead to an establishment of an appropriate diagnostic method for small tissue specimens.

1995 Using Targeted Next-Generation Sequencing to Detect Single Nucleotide Variants, Fusions and Copy Number Variants in Hematologic Malignancies.

Jeremiah Karrs[1], Xiaofei Yu[2], Vernell Williamson[3], Fernanda Charreun[4], Weihua Tang[5], Andrea Ferreira-Gonzalez[6]
[1]Richmond, VA, [2]Virginia Commonwealth University School of Medicine, Richmond, VA, [3]Virginia Commonwealth University, Richmond, VA, [4]Virginia Commonwealth University Health System, Richmond, VA, [5]Henrico, VA, [6]VCU Health, Richmond, VA

Disclosures: Jeremiah Karrs: None; Xiaofei Yu: None; Vernell Williamson: None

Background: As genetic characterization of hematologic malignancies continues to be refined, molecular assays that only survey single nucleotide variants (SNPs) and small genetic changes have become insufficient. We evaluated 48 samples (including clinical samples and controls) utilizing DNA and RNA to investigate SNPs, fusions and copy number variants (CNVs) previously identified by next-generation sequencing (NGS) and FISH to determine the reliability of a using a single assay to detect all three types of genetic alterations.

Design: We extracted DNA and RNA from clinical samples (blood and bone marrow) using Qiasymphony and Trizol extractions respectively; samples were quantitated using Qubit and evaluated for quality using real time PCR (Archer PreSeq QC assays). Serial dilutions were prepared using SeraSeq Myeloid Mutation DNA and SeraSeq Myeloid Mutation RNA. Library preparation was performed using universal and gene specific primers (Archer VariantPlex and FusionPlex) followed by library quantification using real time PCR (Kapa library quantification). The library was sequenced on an Illumina NextSeq instrument ensuring adequate cluster density (130-250), data was converted from BCL to FASTQ format (bcl2fastq) and uploaded onto the Archer Analysis (version 6.0) web based platform for bioinformatic processing and data analysis. Custom settings were applied using alternative observations > 5, unique alternative observations >=3, specific consequences for alterations, allele frequency >0.027, gnomAD frequency <=0.05, use of three variant calling algorithms (FreeBayes, Vision, LoFreq) and disallowing sequence directional bias.

Results: We detected 62/63 SNPs, 16/16 fusions and 4/4 CNVs. The positive predictive accuracy was 98.4% and the positive predictive value was 100.0%. We detected fusions down to 3.4% of reads in dilutions with wild type RNA and SNPs down to 2.73% in wild type DNA using serial dilutions. Copy number variants were detected down to loss of both copies or as high as 12 copies.

Fusion (% total reads)	No dilution	1:2 Dilution	1:4 Dilution
BCR-ABL1	43.8	19.5	8.9
RUNX1-RUNX1T1	44.4	37.5	33.1
FIP1L1-PDGFRA	93.4	95.1	91.6
ETV6-ABL1 (Isoform 1)	5.9	3.5	1.6
TCF3-PBX1	8.3	8.9	2.3
ETV6-ABL1 (Isoform 2)	6.7	2.7	1.9
PML-RARA	6.6	3.7	1.2
KAT6A-CREBBP	24.5	21.7	8.8
PCM1-JAK2	3.4	Not Detected	Not Detected
SNV (% allele frequency)	No Dilution	1:2 Dilution	1:4 Dilution
ABL1 Thr315Ile	16.27	7.72	2.95
ASXL1 Glu635ArgfsTer15	8.04	3.65	1.27
ASXL1 Gly646TrpfsTer12	9.23	5.65	3.16
BRAF Val600Glu	23.83	10.14	2.55
CBL Leu380Pro	18.35	10.66	2.96
CBL Arg420Gln	22.07	10.05	2.86
CEBPA Lys313Dup	12.75	5.97	2.37
CEBPA His24AlafsTer84	5.56	3.23	0.85
CSF3R Thr618Ile	8.47	5.38	0.84
FLT3 Asp835Tyr	15.42	6.42	2.27
IDH1 Arg132Cys	6.39	4.34	1.41
JAK2 Asn542_Glu543del	13.73	8.15	1.9
MPL Trp515Leu	8.8	3.42	1.86
MYD88 Leu265Pro	13.64	7.76	2.56
SF3B1 Lys700Glu	10.21	4.42	2.06
SF3B1 Lys666Asn	5.36	2.73	Not Detected
SRSF2 Pro95_Arg102del	5.86	3.18	Not Detected
U2AF1 Ser34Phe	16.19	8.84	2.27

Figure 1 - 1995

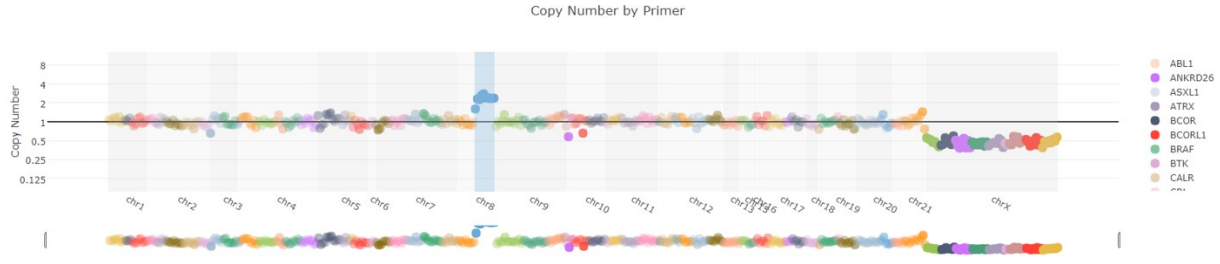

Figure 2 - 1995

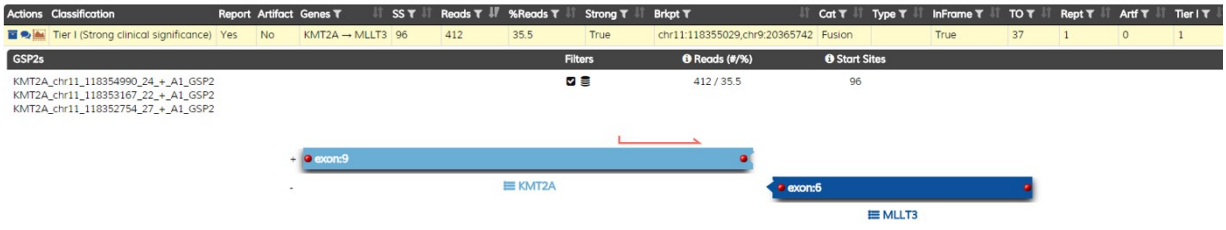

Conclusions: Based on our current findings, using a targeted NGS panel with a refined bioinformatic pipeline that investigates DNA and RNA changes in a single assay, we have been able to match what previously took multiple tests at our institution. Moving forward, we expect to refine our findings, clinically validate the assay and also use it for research.

1996 Predicting Advanced Liver Fibrosis through a Deep Learning-Based Image Analysis Approach

Sergey Klimov[1], Alton Farris[2], Chen Yaobing[3], Hao Chen[4], Yi Jiang[4]
[1]Roswell, GA, [2]Emory University, Atlanta, GA, [3]Tongji Hospital, Tongji Medical College of Huazhong University of Science and Technology, Wuhan, China, [4]Georgia State University, Atlanta, GA

Disclosures: Sergey Klimov: None; Alton Farris: *Grant or Research Support*, MedImmune, Inc.; Chen Yaobing: None; Yi Jiang: None

Background: Liver fibrosis results from chronic liver damage and has been a strong clinical indication for liver health. Identifying the progression of liver fibrosis is vital for therapy recommendation and management. Liver fibrosis staging is often performed by expert

pathologists using stains that target extracellular matrix components such as collagen; such analysis may be hindered by staining and interpretation variability. This study aimed to provide a more accurate and automated fibrosis classifier by machine learning analysis of features obtained from full slide H&E images.

Design: High-resolution, stage-annotated, H&E images (n = 115) were analyzed using a two-fold classification pipeline. First, a trained (through matched Masson's trichrome slides) pixel-based deep learning classifier (LinkNet) was used to perform sematic segmentation to annotate practical domains (collagen (C), lumen (L), non-collagen (NC)) (Fig. 1). Next, 37 full-slide features stemming from these annotations, which represented quantitative fibrotic descriptors such as fibrotic branching, envelopment, and fiber alignment, were developed and compared between patients with cirrhosis (S4) and all others (S0-S3). Finally, 10-fold cross-validated feature and machine learning algorithm selection was used to identify the optimal cirrhosis classifier, which was compared against the Masson trichrome stain's positive pixel count.

Results: On 51 million ground truth pixels, the pixel-based classifier leveled off at a prediction accuracy of over 99%. Individual full-slide features varied significantly in stage discrimination, with area under the curves (AUC) ranging between 0.70 and 0.93. Using only 3 whole slide H&E features, an optimized Support Vector Machine (SVM) model produced a cross validated sensitivity of over 86% and a 95% specificity for S4 (as compared to 52% and 96% respectively, using the trichrome stained positive pixel count) (Table 1).

Table 1. Performance Metrics for Stage 4 Prediction using the Proposed Machine Learning Model or the Trichrome Positive Pixel Count

	Proposed Model	Trichrome Positive Predicted Pixels
Sensitivity	0.86	0.52
Specificity	0.95	0.96
Accuracy	0.93	0.88
AUC	0.96	0.83

Figure 1 - 1996

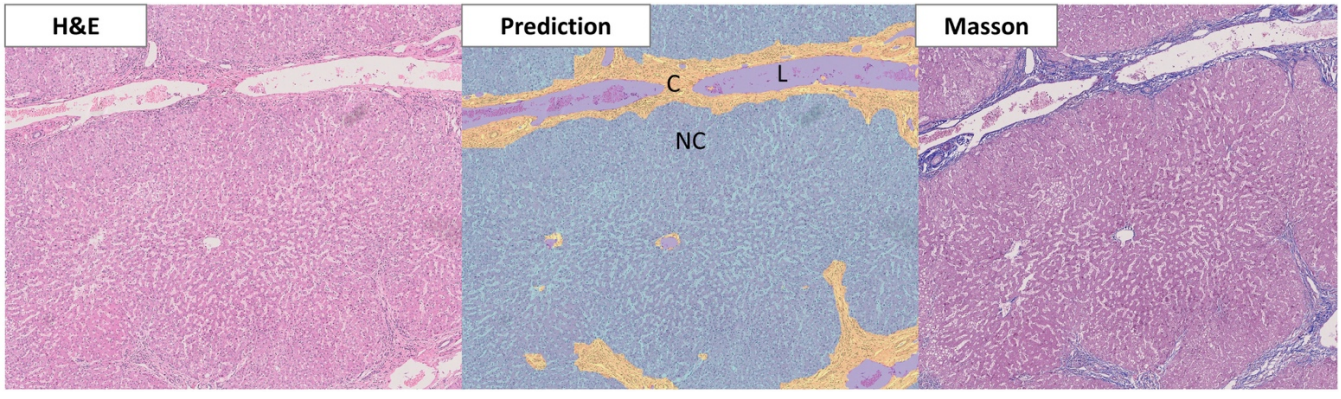

Conclusions: Our novel, two-fold, H&E-based classification model provides a high degree of confidence in cirrhosis prediction for liver biopsies, showing superior prediction compared to Masson trichrome-based metrics. Thus, our model can be used to both supplement current pathological analysis and be used confidently for rapid biopsy staging where only H&E slides may be available.

1997 Mapping the Binding Sites of Antibodies Used in Programmed Cell Death Ligand-1 (PD-L1) Diagnostic Tests

N Lawson[1], Carly Dix[2], Paul Scorer[1], C.J. Stubbs[3], E. Wong[2], Liam Hutchinson[4], E. McCall[2], M. Schimpl[3], E. De Vries[2], J. Walker[5], G.H. Williams[6], James Hunt[2], Craig Barker[1]
[1]Precision Medicine Laboratories, Precision Medicine and Genomics, IMED Biotech Unit, AstraZeneca, Cambridge, United Kingdom, [2]Discovery Biology, Discovery Sciences, IMED Biotech Unit, AstraZeneca, Cambridge, United Kingdom,[3]Structure, Biophysics and Fragment-Based Lead Generation, Discovery Sciences, IMED Biotech Unit, AstraZeneca, Cambridge, United Kingdom, [4]Spirogen, MedImmune, London, United Kingdom, [5]Oncology Companion Diagnostics Unit, Precision Medicine and Genomics, IMED Biotech Unit, AstraZeneca, Cambridge, United Kingdom, [6]Oncologica UK Ltd., Cambridge, United Kingdom

Disclosures: N Lawson: *Employee*, AstraZeneca; Carly Dix: None; Paul Scorer: *Employee*, AstraZeneca; Liam Hutchinson: None; E. McCall: None; J. Walker: *Employee*, AstraZeneca Pharmaceuticals LP; G.H. Williams: *Grant or Research Support*, AstraZeneca Pharmaceuticals LP; James Hunt: *Employee*, AstraZeneca; Craig Barker: *Employee*, AstraZeneca

Background: PD-L1 expression level in patient tumor samples has proven clinical utility across a range of cancer types. A number of independently-developed PD-L1 immunohistochemical (IHC) diagnostic tests are commercially available. Published studies using SP263, SP142, 22C3, 28-8 and E1L3N assays have demonstrated differing levels of PD-L1 concordance between assays, resulting in conjecture as to whether antibody binding epitopes are responsible for discordances. To understand the performance of different PD-L1 diagnostic assays, it is important to understand whether the antibodies used in these tests recognize similar or different epitopes within the PD-L1 protein.

Design: The sites at which clones SP263, SP142, 22C3, 28-8 and E1L3N bind to recombinant PD-L1 was assessed using a range of methods, including Chemical Linkage of Peptides onto Scaffolds (CLIPS), Surface Plasmon Resonance (SPR) and/or Hydrogen Deuterium Exchange Mass Spectrometry (HDX-MS). Putative binding sites were confirmed by site-directed mutagenesis of PD-L1, followed by Western blot and IHC analysis of cell lines expressing mutant constructs.

Results: Clones 22C3 and 28-8 have binding profiles in the extracellular domain of PD-L1, different from one another. Clones SP263 and SP142 bind to an identical epitope in the cytoplasmic domain at the extreme C-terminus of PD-L1, distinct from 22C3 and 28-8. Using mutated PD-L1 constructs an additional clone, E1L3N, was also found to bind the cytoplasmic domain of PD-L1. The E1L3N binding epitope overlaps significantly with the SP263/SP142 binding site but is not identical.

Conclusions: Our results demonstrate that clones SP263, SP142 and E1L3N bind similar or identical epitopes within the cytoplasmic domain of PD-L1, whereas clones 22C3 and 28-8 bind to different epitopes in the extracellular domain. Despite identifying epitope binding variance between antibodies, assay concordance studies indicate that only the SP142 assay generates substantially discordant IHC staining. This is unlikely to be related to the epitope, as it is identical to that for SP263; but more likely due to the protocol, which can be modified to produce staining comparable to the other assays. It is more likely that inter-assay discordances are attributable to tumor heterogeneity, assay or platform variables rather than antibody epitope.

1998 Whole Mount Grossing of Whipple Specimens: Histology Techniques and Outcomes

Valerie Lockhart[1], Nicole Tomsho[2], Angela Bitting[2], Erin Powell[2], Jeffrey Prichard[1], Fan Lin[2]
[1]Geisinger, Danville, PA, [2]Geisinger Medical Center, Danville, PA

Disclosures: Valerie Lockhart: None; Nicole Tomsho: None; Angela Bitting: None; Erin Powell: None; Jeffrey Prichard: None; Fan Lin: None

Background: Due to the revision of the (exocrine) pancreatic cancer staging system in the 8th edition of the AJCC Cancer Staging Manual, our institution began using a whole mount (WM) method to gross Whipple specimens using axial slicing techniques, cutting from superior to inferior, to identify the tumor with key anatomic structures/relationships intact, more accurately determine tumor size, assess the entire circumferential margin, identify more lymph nodes, and better correlate with CT/MRI findings. Histology procedures were altered to accommodate the whole mount slides, and immunohistochemical (IHC) stains were performed using an automated stainer after the area of interest (AOI) was marked on the WM slide, the corresponding tissue was cut away and re-embedded in a standard-sized mold, and standard-sized slides were made (Figure 1).

Design: CoPath reports and Quality Assurance (QA) Tracker data were reviewed for all 44 Whipple specimens grossed using the WM method from August 2017 to September 2018. The IHC turnaround time (including the extra steps of identifying/isolating the AOI, re-embedding the tissue, and cutting standard-sized slides) and quality data were analyzed.

Results: IHC was ordered on 8 of 44 WM cases for a total of 24 IHC stains performed on 10 different blocks. All 24 IHC stains had a turnaround time of less than 24 hours. Three of 44 cases had a total of five reported quality issues. Three issues were reported during processing (inadequate fixation—2, sections too thick—1), and two issues were reported by pathologists (stain too pink—1, whole mount sections not intact and need to be recut—1). The other 93.2% of whole mount cases did not have any reported quality issues.

Figure 1 - 1998

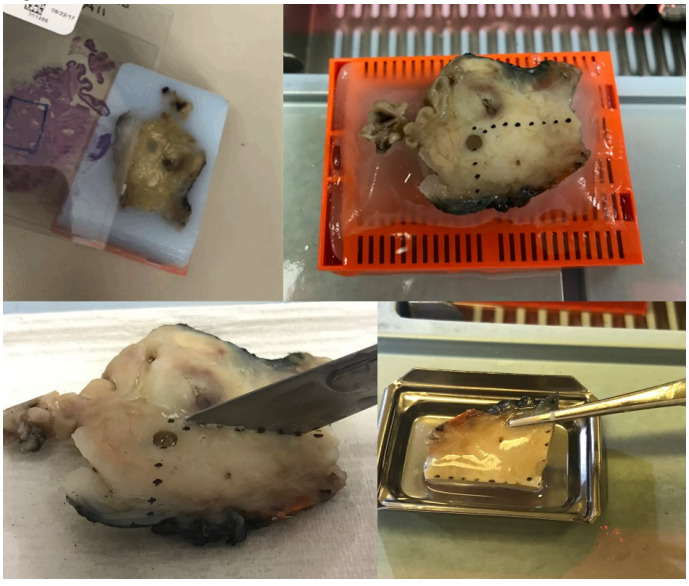

Conclusions: The 100% IHC turnaround time of less than 24 hours, which is the expected turnaround time for IHC stains at our institution, indicates that our IHC processing techniques are efficient and adequate. The great majority of the WM cases did not have quality issues (93.2%), and four of the five quality issues were reported within the first 8 cases that were grossed using the WM technique. The latter 36 cases had a quality issue rate of only 2.8%. This suggests that quality improved over time as the histotechs gained more experience processing these specimens.

1999 Chromosome Microarray Analysis for Morphologically Challenging Renal Neoplasms

Sundis Mahmood[1], Joel Lefferts[2], Jason Pettus[1], Jorge Gonzalez[1], Bing Ren[3]
[1]Dartmouth Hitchcock Medical Center, Lebanon, NH, [2]Lebanon, NH, [3]Dartmouth-Hitchcock Medical Center, Lebanon, NH

Disclosures: Sundis Mahmood: None; Bing Ren: None

Background: Renal cell carcinoma (RCC) is a relatively common malignancy with significant worldwide annual mortality. However, the prognosis and treatment may vary widely among RCC histologic types, highlighting the critical task of proper classification by pathologists. Although combined histology and immunohistochemistry (IHC) allows for classification of most RCC's, a proportion of cases defy classification. Since some subtypes of RCC display reproducible chromosomal abnormalities, our laboratory has employed chromosomal microarray analysis (CMA) for challenging cases. CMA is a genomic tool that provides genome-wide copy number information from DNA isolated from various specimens, including formalin fixed paraffin-embedded (FFPE) tissue.

Design: Oncoscan CNV (ThermoFisher) is a SNP-based CMA assay that uses molecular inversion probes to interrogate over 220,000 single nucleotide polymorphisms (SNPs) throughout the genome with coverage focused on cancer-related genes. In addition to changes in copy number, copy-neutral loss of heterozygosity (LOH) can also be detected in a timely manner. Oncoscan CNV is being used in real-time to complement morphologic and IHC data for difficult-to-classify renal tumors in an academic genitourinary pathology practice.

Results: Within eleven patients, thirteen morphologically challenging renal tumors were assessed by Oncoscan CNV, all of which yielded interpretable data. Specimen types included ten nephrectomies, two core biopsies, and one fine needle aspirate. Based on prior published literature, identified chromosomal changes were supportive of clear cell RCC (CCRCC) in 3 lesions, mucinous tubular and spindle cell carcinoma (MTSCC) in 3 lesions, and papillary RCC (PRCC) in 1 lesion. Changes of uncertain significance were seen in 5 lesions, including an oncocytoma with sinus fat extension showing losses of chromosomes 18 and 19. Lastly, a TFE translocation carcinoma (confirmed by fluorescence in situ hybridization) showed no detectable changes by CMA.

Patient	Gender/Age	Specimen type	Diagnosis based on morphology and IHC	CMA	Final Diagnosis
1	F/52	FNA	High grade RCC	LOH: ch 1, 4, 6, 8, 9, 13, 14, 15, 18, and 22.	MTSRCC with sarcomatoid transformation
2	F/32	Partial nephrectomy	RCC NOS	Loss: ch 1, 6, 11q, 15q, 22q	MTSRCC
3	F/47	Radical Nephrectomy	RCC NOS	Loss: ch 1, 4, 6, 8, 9, 11, 13, 14, 15, 22 and X	MTSRCC
4	M/50	Radical Nephrectomy	Eosinophilic RCC NOS	Gain: ch 3q, 5p, 5q, 8q, 12 Loss: ch 3p, 8p, 13, 14, 18, Y	Clear cell RCC
5	M/33	Retroperitoneal lymph node biopsy	Malignant neoplasm, compatible with renal origin.	Gain: ch 1p, 1q and 5q Loss: ch 3p, 6p, 8p, 9, 13q, 14q, 15q, 17p, 21q, 22q LOH: ch 1q and 11p	Clear cell RCC with sarcomatoid differentiation
6	M/56	Radical nephrectomy	Acquired cystic disease associated RCC vs papillary RCC	Gain: ch 3, 7, 12, 16, 17, and 20	Papillary RCC
7	M/80	Radical nephrectomy	Mass # 1 – Clear cell RCC	Mass # 1 - Gain: ch 5q Loss: ch 3p	Mass # 1 – Clear cell RCC
			Mass # 2 - Eosinophilic RCC, favor oncocytoma	Mass # 2 – Gain: ch 17q, 20p	Mass # 2 - RCC NOS, chromosomal alteration with uncertain significance
8	M/70	Partial nephrectomy	Eosinophilic RCC NOS, favor papillary RCC	Gain: ch 5, 13 and 18 Loss: ch 9, 14 and 15	RCC NOS, chromosomal alteration with uncertain significance
9	M/67	Biopsy	High grade RCC	Gain: ch 3q, 8q	RCC NOS, chromosomal alteration with uncertain significance
10	F/64	Radical nephrectomy	Mass # 1 – Acquired cystic disease associated RCC	Mass # 1 – No alteration	Mass # 1 – TFE3 translocation-associated RCC (confirmed by FISH)
			Mass # 2 – Acquired cystic disease associated RCC with oncocytoma features	Mass # 2 - Gain: ch 5, 13, 16, and 17 Loss: ch 22 LOH: ch 7	Mass # 2 - Tubulo-cystic renal cell carcinoma (outside consultation diagnosis), chromosomal alteration with uncertain significance
11	F/63	Radical nephrectomy	Atypical oncocytoma	Loss: ch 18, 19	Oncocytoma with unusual chromosomal alteration

Note: RCC, renal cell carcinoma; NOS, not otherwise specified; LOH, loss of heterozygosity; MTSRCC, mucinous tubular and spindle renal cell carcinoma; ch, chromosome; IHC, immunohistochemistry; CMA, chromosome microarray analysis; FISH, fluorescence in situ hybridization.

Conclusions: Specific classification of renal neoplasms is critical to ensure appropriate patient prognostication and therapy. Oncoscan CNV chromosomal microarray technology has proven to yield reliable results, even for very small tissue samples, which may be more clinically useful than FISH for assessing recurrent chromosomal abnormalities of morphologically challenging renal neoplasms. In this small proof-of-principle series, we were able to more accurately support a specific diagnosis in 8 of 13 (62%).

2000 Multiple Calcifying Fibrous Pseudotumors of the Thoracic Pleura: Ultrastructural Analysis Provides Insight on Mechanism of Dissemination

Lucas Massoth[1], Ivan Chebib[2], Richard Kradin[1]
[1]Boston, MA, [2]Massachusetts General Hospital, Harvard Medical School, Boston, MA

Disclosures: Lucas Massoth: None; Ivan Chebib: None; Richard Kradin: None

Background: Calcifying fibrous pseudotumor (CFP) is a rare, benign soft tissue tumor that can appear in a variety of locations, most often as a solitary mass. It is characterized by benign-appearing fibroblasts within dense fibrocollagenous tissue, psammomatous calcifications and focal lymphoplasmacytic inflammation. These tumors may arise in the pleura and often show multifocal dissemination across the pleural surface, but the mechanism underlying this dissemination is unclear. We present a 59-year-old male with multiple CFP of the thoracic pleura. Reactive-appearing adhesions spanning the pleural surfaces were present and, by electron microscopy, were involved by tumor.

Design: Clinical, radiologic and histopathologic features were reviewed and a panel of immunohistochemical stains were performed. Transmission electron microscopy of the tumor and pleural adhesions was performed from formalin-fixed paraffin-embedded tissue.

Results: Microscopy of CFP revealed hyalinized fibrocollagenous tissue with interspersed benign-appearing fibroblasts, areas of lymphoplasmacytic inflammation, and psammomatous calcifications. Cross-sections of associated adhesions demonstrated collagenous tissue involved by lymphoplasmacytic inflammation and were surfaced by normal appearing mesothelium. Von Kossa stain identified minute calcifications within adhesions.

Electron microscopy of solid tumor revealed a striking pattern of haphazard collagen arrangement. Pleural adhesions demonstrated a normally arranged sub-mesothelial collagen layer transitioning to increasingly disorganized central collagen, merging with the haphazard pattern present within the tumor. Foci of ultrastructural calcium deposition on collagen fibrils were identified within the adhesion.

A literature review identified 19 other cases of pleural CFP. Including the current case, 14 (70%) showed tumor multifocality. Seven cases documented adhesions, tumor arborization, and/or tumors suspended between the pleural surfaces.

Conclusions: Pleural CFP may present in disseminated fashion across the pleural surfaces. Other reported cases in the literature have described coincident adhesions, tumor arborization, and suspended tumors. Ultrastructural examination of the adhesions in the present case revealed characteristic findings of CFP, including haphazardly organized collagen and early calcifications. Tumor involving the adhesions appear to represent the mode of dissemination across and between the pleural surfaces, leading to multifocality.

2001 Exploring Morphological Biomarker for Predicting Responsiveness to the Immune Checkpoint Inhibitor Therapy using Whole-Slide Digital Images of Non-Small Cell Lung Cancer

Noriko Motoi[1], Hiroshi Yoshida[1], Tomoharu Kiyuna[2], Hiroyasu Saiga[2], Yoshiko Yamashita[3], Takashi Kohno[4], Yuichiro Ohe[5], Atsushi Ochiai[6]
[1]National Cancer Center Hospital, Chuo-ku, Japan, [2]Future City Development Division, NEC Corporation, Minato-ku, Japan, [3]Corporate Business Development Division, NEC Corporation, Minato-ku, Japan, [4]National Cancer Center Research Institute, Tokyo, Japan, [5]National Cancer Center Hospital, Tokyo, Japan, [6]National Cancer Center, Kashiwanoha, Kashiwa, Japan

Disclosures: Noriko Motoi: None; Hiroshi Yoshida: None; Tomoharu Kiyuna: None; Yoshiko Yamashita: None

Background: As for eligible patients' selection for immune check point inhibitor therapy (ICI), PD-L1 IHC is feasible but not a perfect biomarker. We hypothesized that morphological characteristics should reflect genetic alteration, thus could predict ICI responsiveness. In this study, we examined predictive potential of morphological characteristics using digital whole-slide images as a new biomarker for ICI-treatment on non-small cell lung cancer (NSCLC) and their relationship to PD-L1 IHC and genetic alterations.

Design: 47 NSCLC who received ICI therapy were recruited. Digital images of HE and PD-L1 (22C3) IHC stained slides of pre-treatment biopsied or resected materials were examined by previously reported image analysis techniques (Ref. Gastric Cancer. 2018 Mar;21(2):249-257. Oncotarget. 2017 Oct 31; 8(53): 90719–90729.) Morphological characteristics of cancer cells (three and six parameters of nuclear shape and of chromatin texture) were elicited as MC-scores. Tumor mutation burden (TMB) were examined by the NGS-based target sequence (NCC oncopanel ®). Correlation between morphological characteristics and clinical outcome and TMB status was calculated. We explored the predictive MC-score as well as a decision tree model for ICI-responsiveness. P value less than 0.05 was considered as statistically significant. Decision tree model was built using statistically significant factors.

Results: Of the responders, the following MC-score of cancer cell were statistically different from those of the responders; nuclear size (larger, $p<0.001$), circularity (more circular, $p<0.001$) and nuclear contrast (higher contrast, $p<0.001$). Circularity ($p=0.011$) and texture

homogeneity (p=0.048) correlated with TMB. Angular second moment (ASM) texture correlated with PD-L1 expression (p=0.018). The decision tree model for predictive and screening purposes resulted 0.83 and 0.62 accuracy, respectively.

Conclusions: Our results indicate the substantial value of morphological feature as a biomarker for ICI therapy. Morphological characteristics are elicitable from archived FFPE samples, showed good correlation to the underlying genetic alteration.

2002 Unsaturated Lipids as Spectral Marker for Objective Discrimination of Breast Cancer Cells (MCF-7) From Normal Human Mammary Epithelial Cells (HMEpC) in Raman Microspectroscopy (RM)

Hemanth Noothalapati[1], Keita Iwasaki[2], Riruke Maruyama[3], Asuka Asuka[4], Tatsuyuki Yamamoto[1]
[1]Raman Center for Medical and Biological Applications, Shimane University, Matsue, Japan, [2]Shimane University, Matsue, Japan, [3]Izumo, Japan, [4]Shimane University, Faculty of Medicine, Izumo, Japan

Disclosures: Hemanth Noothalapati: None; Keita Iwasaki: None; Riruke Maruyama: None; Asuka Asuka: None; Tatsuyuki Yamamoto: None

Background: Conventional cytology is easy to perform and relatively non-invasive. However, there are a certain number of indeterminate cases even when it is expected to play a critical role in making a therapeutic decision. Application of RM in cytology as an adjunct to morphology is anticipated to solve such a problem, particularly because it is a non-invasive, label-free method that provides rich chemical information. However, two major concerns should be addressed before introducing RM in clinics: 1) concrete knowledge of molecular changes in cells must be established and 2) screening of spectral markers that are unaffected by the choice of instrument, especially excitation wavelength, is necessary for universal adoption of this technique.

Design: To address above mentioned concerns, a two-fold experiment was designed. First, 633nm excited Raman spectra were obtained from 30 independent HMEpC and MCF-7 cells. Each spectrum is an average of 5 random points in a cell. Data from all 60 cells were then analyzed together. Both conventional univariate approach and multivariate statistical methods were utilized to model Raman spectra. Especially, by employing multivariate curve resolution analysis (MCR), we succeeded in extracting pure biochemical components from complex cellular data and their relative abundances were used to elucidate the underlying molecular changes in cancer cells. Then we repeated the whole process (measurement and analysis) with 532nm excited Raman spectra to screen for spectral markers independent of excitation wavelength.

Results: MCR analysis of 633nm excited Raman hyperspectral data with non-negative constraints led us to identify 5 physically meaningful pure biochemical spectra comprising DNA, proteins and surprisingly 3 lipid components (Fig. 1A). Lipid 1 is assigned to di-unsaturated fatty acid while other 2 components correspond to mono-unsaturated lipids. Intriguingly, ratio of total DNA / Lipid 1 (Fig. 1B) and Protein / Lipid 1 (Fig. 1C) are strictly regulated (HMEpC << MCF-7) and can be used for objective discrimination of cancer cells from normal cells. Moreover, results of MCR analysis of 532nm excited data revealed similar lipid profiles (Fig. 2A). Biomolecular ratios (Fig. 2B & C) also corroborate well supporting our proposal to use unsaturated lipids as spectral hallmark to discriminate breast cancer cells.

Figure 1 - 2002

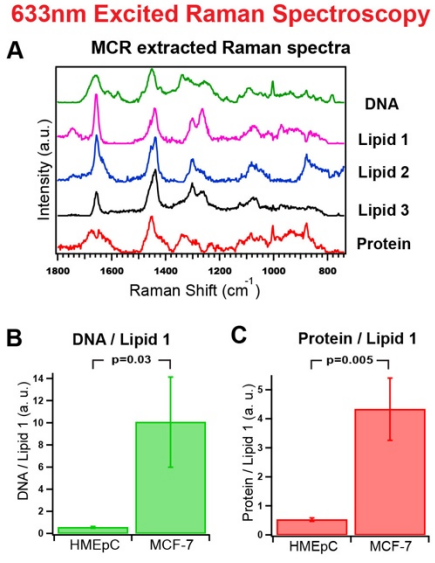

Figure 2 - 2002

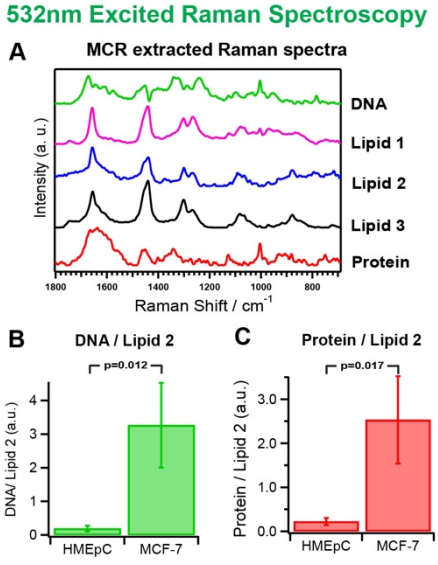

Conclusions: RM has the potential to become an excellent cytodiagnostic tool that can both accurately and objectively discriminate cancer from normal cells.

2003 BRAF Mutation Testing of Pigmented Melanomas using the Idylla Platform

Danielle Petty[1], Omer Hassan[1], Callie Barker[1], Stacey O'Neill[1]
[1]Wake Forest Baptist Medical Center, Winston Salem, NC

Disclosures: Danielle Petty: None; Omer Hassan: None; Callie Barker: None; Stacey O'Neill: None

Background: *BRAF* mutations are present in ~50% of all melanomas and targeted therapy has been associated with improvement in overall and progression-free survival. Timely assessment of mutation status is important for clinical decision making. Melanomas with high melanin content can be problematic for molecular assays due to inhibition of PCR. We evaluated *BRAF* mutation testing using the Idylla platform from Biocartis. This platform has recently been introduced into the United States, and offers cartridge-based testing for concurrent BRAF V600E/E2/D and V600K/R/M mutation detection with minimal hands-on time and low sample input requirement.

Design: Twenty-three FFPE melanoma samples from our medical center with known *BRAF* mutation results from reference lab testing were retrospectively identified. Cases included cytology cell blocks (8), small biopsies (4), and excisional biopsies/resection specimens (10). During pathologist review of H&E stained slides, pigment scores were rendered as 0 (no pigment, n=5), 1 (moderate pigment, n=10), or 2 (abundant pigment, n=7). This sample cohort included 14 *BRAF*mutation positive and 7 mutation negative samples. Testing on the Idylla platform was compared to reference lab testing for sensitivity and specificity. Reproducibility, limit of detection, and melanin interference were also evaluated.

Results: Sensitivity and specificity of *BRAF* mutation detection were 100% as compared to reference lab testing in 21 samples. Abundant melanin did not inhibit the assay, as demonstrated by samples with a pigment score of 2 successfully resulted. Tissue input requirement was low, with a single 5 ?m section tested for small biopsies and resections. Cell block material with as few as ~400 tumor cells in the background of red blood cells was successful in detecting BRAF V600E. Two samples in this cohort contained insufficient DNA for testing, including one cell block and one needle core biopsy. Results were reproducible, and as little as 1% mutant allele of V600E and V600K was detected using Horizon Discovery control material. The assay required only 10-15 minutes of total hands-on time and the instrument time was ~90 minutes, including extraction.

Conclusions: *BRAF* mutation assay on the Idylla platform provides robust testing for melanomas with high melanin content, including limited cytology cell block material. Total assay time of <2 hours facilitates prompt results to guide patient care decisions.

2004 Muse (Microscopy with UV Surface Excitation), A Slide-Free Technique to Evaluate Surgical Pathology Specimens

Amir Qorbani[1], Nicole Dawson[2], Mitchell Moosavi[3], Roshanak Alialy[4], Farzad Fereidouni[5], Austin Todd[5], Steven Hart[6], Pasathorn Potivongsajarn[3], Chayanit Jumniensuk[3]
[1]University of California, Los Angeles, Marina Del Rey, CA, [2]David Geffen School of Medicine at UCLA, Santa Monica, CA, [3]University of California, Los Angeles, Los Angeles, CA, [4]New York, NY, [5]University of California, Davis, Sacramento, CA, [6]Los Angeles, CA

Disclosures: Amir Qorbani: None; Nicole Dawson: None; Mitchell Moosavi: None; Roshanak Alialy: None; Farzad Fereidouni: None; Austin Todd: None; Steven Hart: None; Pasathorn Potivongsajarn: None; Chayanit Jumniensuk: None

Background: MUSE is a novel ex-vivo microscopy technique that employs ultraviolet light- excitation of common fluorescent tissue dyes within about 10 microns of the surface of fresh or fixed specimens. The method requires about 2 minutes of sample preparation and generates full-color, high-resolution images at 200 msec per 1mm^2; these can be color-converted to resemble H&E. The MUSE procedure does not harm the tissue for future use in the traditional H&E preparation or molecular testing. The aim of this study was to evaluate MUSE on a wide range of surgical pathology cases.

Design: 20 samples of different surgical pathology cases (kidney, thyroid, intestine, breast, prostate, lung, liver and skin) evaluated by six board-certified pathologists and three pathology residents after brief training. For each case, “Diagnostic Score” (% of correct answers) and “Comparison Scores” (0: Not useful/ 1: useful but not diagnostic / 2: diagnostic but weaker than H&E / 3: Equal to H&E / 4: Stronger than H&E) were determined by comparing the MUSE images with the corresponding conventional FFPE-H&E images generated by whole-slide scanning.

Results: Results indicate that MUSE is a promising modality for histopathology, generating an average diagnostic score of 80% and a comparison score of 2.4.

Figure 1 - 2004

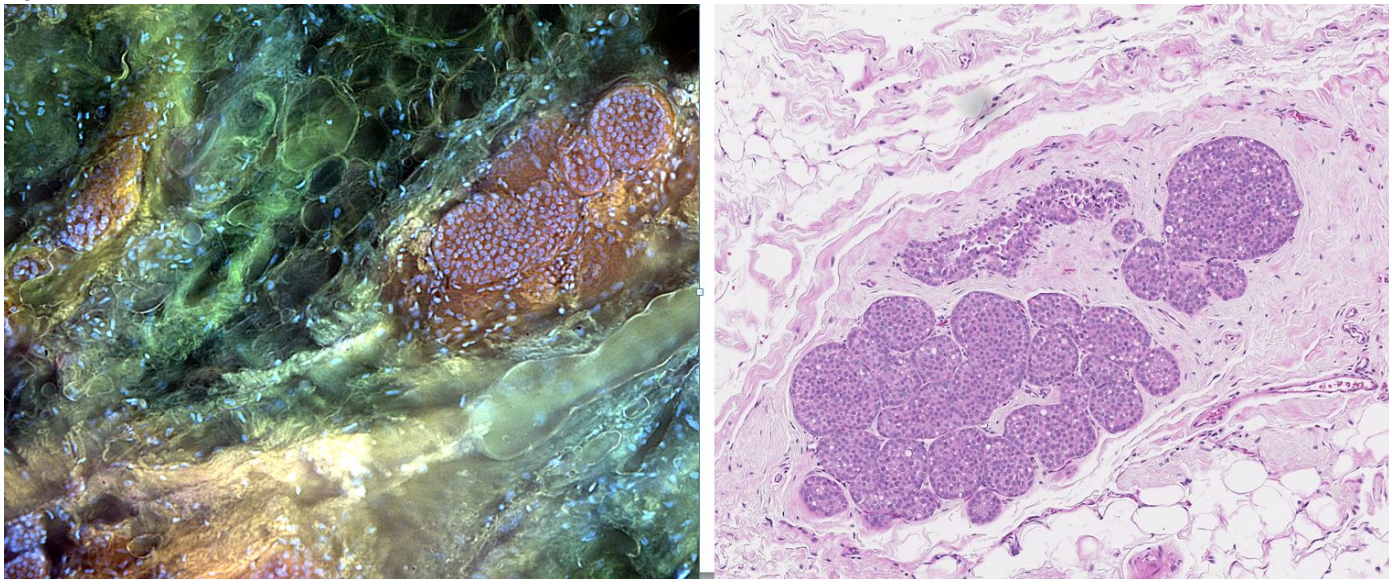

Figure 2 - 2004

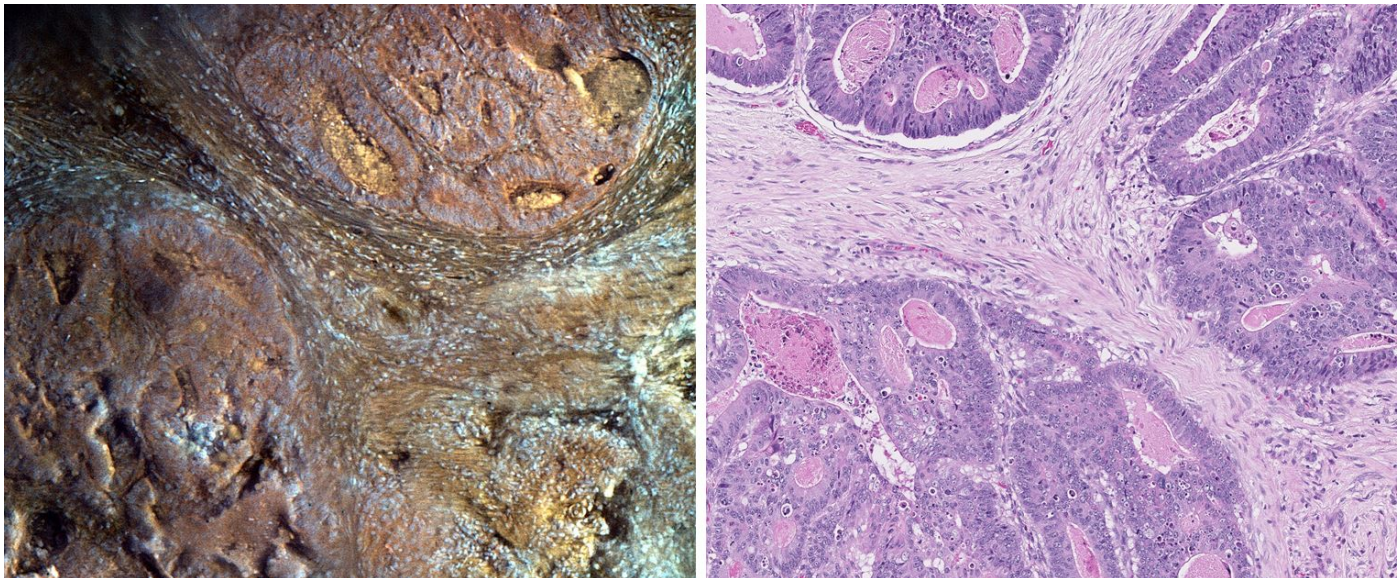

Conclusions: MUSE represents a fast, reliable and inexpensive approach for evaluating surgical specimens. It could be a useful diagnostic tool, but in the implementation used here appears to be slightly weaker than H&E on providing all necessary histologic details. Going forward we continue to evaluate the application of MUSE in different clinical settings particularly in intraoperative consultations.

2005 Image Mass Cytometry to Detect Immune Cells and Predictive Biomarkers in Formalin-Fixed and Paraffin-Embedded Tissue

Yasmeen Rizvi[1], Jared Burks[1], Duncan Mak[1], Funda Meric-Bernstam[1], Coya Tapia[1]
[1]The University of Texas MD Anderson Cancer Center, Houston, TX

Disclosures: Yasmeen Rizvi: None; Jared Burks: None; Duncan Mak: None; Funda Meric-Bernstam: *Advisory Board Member*, Inflection Biosciences, Spectrum Pharmaceuticals; *Consultant*, Sumitomo Group, Dialectica, Genentech, Pieris Pharmaceuticals, Clearlight Diagnostics, Darwin Health, Samsung Bioepis, Aduro Biotech, Origimed, Xencor, Debiopharm Group; *Grant or Research Support*, Novartis, AstraZeneca, Taiho Pharmaceuticals, Genentech, Calithera Biosciences, Debiopharm Group, bayer, Aileron Therapeutics, PUMA Biotechnology, CytomX Therapeutics; *Grant or Research Support*, Jounce Therapeutics, Zymeworks, Curis, Pfizer, eFFECTOR Therapeutics, Abbvie, Boehringer Ingelheim; Coya Tapia: None

Background: Background: An increasing number of biomarkers need to be evaluated on limited tissues, such as e.g. small biopsies, in the near future to evaluate eligibility for cancer treatment. Hence, one by one testing will reach its capacity limits and so, high multiplex methods will be needed to satisfy the increasing demand for immune profiling and predictive biomarker evaluation. Image mass cytometry (IMC) is a platform that is able to detect >50 proteins in one slide of formalin-fixed and paraffin embedded (FFPE) tissue. Here we report our first results on IMC multiplex on immune cells and predictive biomarkers in one single FFPE tissue slide.

Design: IHC protocols for EGFR, Her2, ATM, and Trop2 were established from antibodies that have a carrier-free format option. The carrier-free versions of these antibodies were labeled with 4 different lanthanides using a commercial kit (Maxpar® Flugidim). Then, positive and negative cell lines were stained with IHC and IMC. Additionally, a her2-positive breast cancer (her2-BC) tissue was incubated with an antibody mix, including CD8, FoxP3, CD68, vimentin, pan-cytokeratin and Ki-67. The additional labeled antibodies were purchased from our flow cytometry and cell imaging core facility and dilutions were used according to manufacturer's website. For visualization of IMC stains the MCD Viewer (Fluidigm) was used.

Results: IMC stains could not be visualized with ATM and Trop2. Cell lines: Clear membrane staining for EGFR and Her2 were seen in the positive controls and no staining was seen in the negative controls. Her2-BC: Her2 staining was in one area more granular and cytoplasmic in IMC compared to IHC with clear membrane staining in all areas. EGFR was negative with both staining methods. The other markers showed comparable/expected results. IMC images showed a lower resolution compared to IHC images.

Conclusions: IMC and IHC detected a positive and negative protein status for EGFR and Her2 equally but IMC showed in one area a nearly exclusive cytoplasmic staining pattern for Her2. This might be due to the fact that IMC is more dependent on even tissue quality/fixation. Ki-67 and immune cell profiling seemed to be less problematic for IMC. MCD Viewer image resolution would not have allowed detailed evaluation regarding e.g. staining intensity and therefore other image software might be more suitable. IMC is a promising platform for multiplex biomarker evaluation/screening but staining/labeling can be challenging.

2006 Feasibility of Use of DNA Flow Cytometry in Bile Duct Brush Samples

Jessica Rogers[1], Eric Huang[2], Peter Rabinovitch[2], Thomas Small[2], Michael Saunders[2], Paul Swanson[3], Matthew Yeh[4], Yongjun Liu[4]
[1]University of Washington Medical Center, Woodway, WA, [2]University of Washington, Seattle, WA, [3]University of Washington, Bainbridge Island, WA, [4]University of Washington Medical Center, Seattle, WA

Disclosures: Jessica Rogers: None; Eric Huang: None; Peter Rabinovitch: None; Thomas Small: None; Michael Saunders: None; Paul Swanson: None; Yongjun Liu: None

Background: The diagnosis of dysplasia/neoplasia in bile duct brush specimen critically impacts subsequent clinical decision making, risk stratification and management, but the pathologic diagnosis can be challenging. Currently, there are no reliable immunohistochemical methods for confirmative diagnosis. We examine if DNA content by flow cytometry can serve as an ancillary tool in this aspect.

Design: DNA flow cytometry was performed on 20 consecutive bile duct brush samples. Two cases were ultimately excluded from the study, as there were too few cells to obtain accurate DNA content. Concurrent parallel cytology slides prepared from the same brush specimens were reviewed by a single cytopathologist.

Results: Normal DNA content was present in 16 of the 18 samples (89%) included in the study. DNA aneuploidy was found in 2 cases (11%) for which the concurrent cytology slides showed reactive glandular epithelium in one case while the second case showed predominantly mucin with rare bland appearing epithelial cells. All concurrent cytology slides from the 16 cases with normal DNA content were negative for dysplasia/neoplasia after review. In the recent five-year retrospective review of all bile duct brush cytology cases in our institution (n=377), 322 (85%) were interpreted as benign, whereas 56 (15%) were interpreted as positive for dysplasia/neoplasia.

Conclusions: Our results confirm the feasibility of DNA flow cytometry as an ancillary tool in evaluating bile duct brush samples, and concurrent cytology review verifies its potential utility in excluding the presence of dysplasia, using DNA aneuploidy as a surrogate marker.

In support of this concept, our feasibility study found an 89% rate of flow cytometry effectively excluding dysplasia/neoplasia compared to an 85% rate of benign cytology interpretation at our institution historically. The lack of concordance between aneuploidy and morphologic atypia in 2 cases is intriguing, and suggests that DNA analysis may be more sensitive than cytologic evaluation in the identification of dysplasia in small samples. We infer from these findings that a larger prospective analysis of biliary epithelial samples representative of the full spectrum of biliary epithelial dysplasia is warranted.

2007 CD44 Immunohistochemistry in the Differential of Squamous and Urothelial Carcinoma: Lack of Expression Supports a Diagnosis of Urothelial Carcinoma

Neha Varshney[1], Andrew Bellizzi[1]
[1]University of Iowa Hospitals and Clinics, Iowa City, IA

Disclosures: Andrew Bellizzi: None

Background: CD44 is a cell surface glycoprotein with numerous roles in health and disease. CD44 has an established role in the distinction of urothelial carcinoma in situ (CIS) from reactive urothelial proliferations. CD44 is normally expressed by basal urothelial cells and is not expressed by umbrella cells. In reactive urothelium, CD44 expression expands to near full-thickness. Urothelial CIS is CD44-negative. Seeking alternative diagnostic applications for this marker, we hypothesized that CD44 IHC would perform similarly in the distinction of reactive from dysplastic squamous proliferations (given developmental biologic/immunophenotypic overlap between squamous and urothelial mucosa). We piloted CD44 IHC in a series of esophageal squamous dysplasias, and, much to our chagrin, they demonstrated strong, near full-thickness staining, similar to reactive squamous (and urothelial mucosa) (Figure 1). We have subsequently hypothesized that CD44 IHC may be useful in the distinction of squamous cell carcinoma (SCC; CD44-positive) from urothelial carcinoma (UC; CD44-negative).

Design: CD44 IHC was performed on tissue microarrays constructed from 232 SCCs (anus 22, cervix 23, esophagus 14, larynx 18, lung 29, penis 21, skin 21, tongue base 10, tonsil 16, vagina 17, vulva 20, ventral tongue 21) and 43 UCs (bladder). Tumors were arrayed as triplicate 1 mm cores. Intensity (0-3+) and extent (0-100%) of expression were assessed, and an H-score (intensity*extent) was calculated. Two-tail Fisher's exact and Mann-Whitney tests were used with $p<0.05$ considered significant.

Results: CD44 was nearly always (94%) expressed by SCCs, while only just over half (51%) of UCs were CD44-positive ($p<0.0001$). Mean and median H-scores in positive SCCs (176; 175) approached statistical significance ($p=0.0661$) vs. those in UC (139; 110). Data stratified by anatomic site are presented in the Table. Rates of CD44-positivity in SCC anatomic subsets ranged from 82-100%, with most >/=95%. Median H-scores ranged from 110 to 265. The combined tongue base/tonsil group showed weaker expression in positive cases than the combined "all other positive" SCC group ($p=0.022$).

Anatomic Site	CD44 % Positive	Mean (Median) H-score (if positive)
Anus	95% (21/22)	176 (160)
Cervix	96% (22/23)	173 (183)
Esophagus	100% (14/14)	160 (150)
Larynx	94% (17/18)	186 (195)
Lung	86% (25/29)	204 (265)
Penis	100% (21/21)	151 (140)
Skin	95% (20/21)	206 (218)
Tongue base	100% (10/10)	141 (110)
Tonsil	94% (15/16)	141 (127)
Vagina	82% (14/17)	154 (162)
Vulva	100% (20/20)	173 (163)
Ventral tongue	95% (20/21)	191 (220)
Urothelial (bladder)	51% (22/43)	138 (110)

Figure 1 - 2007

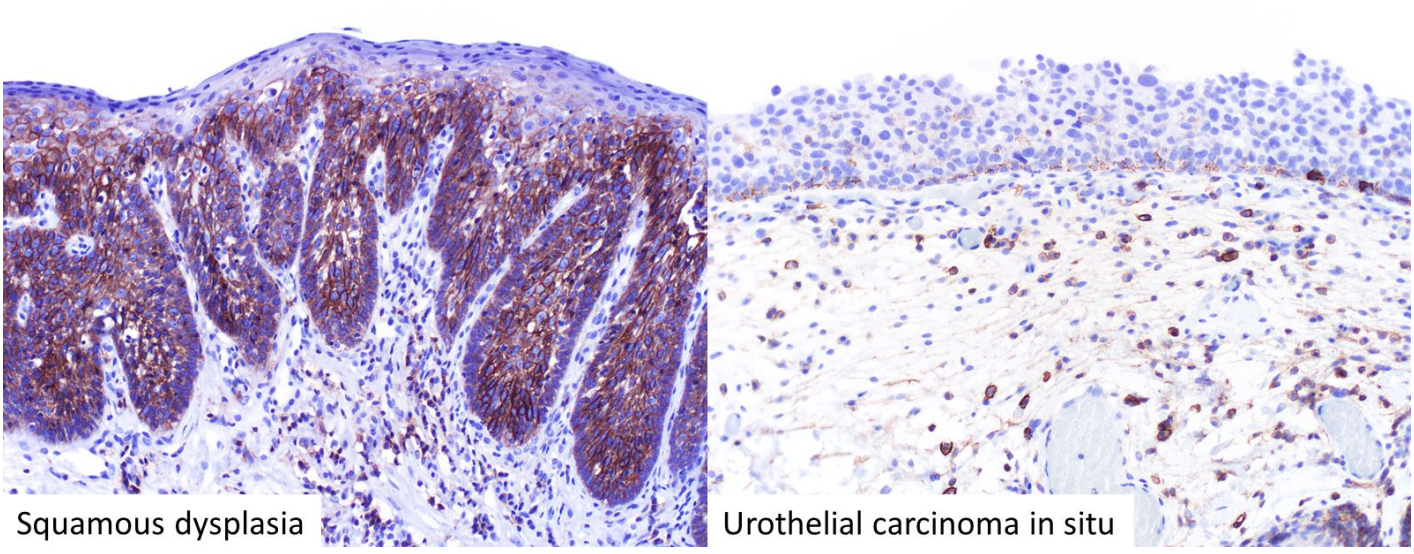

Conclusions: SCCs are nearly always CD44-positive, with expression typically moderate to strong, while half of UCs are CD44-negative. Based on the results of this study, we will employ CD44 in the differential diagnosis of SCC vs UC, with absent staining favoring a diagnosis of UC.

2008 Developing a Robust Sample Preparation Procedure for Deep Fourier-Transform Mass Spectrometric Profiling of Formalin-Fixed Paraffin-Embedded Clinical Tissue Specimens

Yihua Zhou[1], Atsushi Tanaka[1], Ronald Hendrickson[1], Julia Wang[1], Michael H. A. Roehrl[2]
[1]Memorial Sloan Kettering Cancer Center, New York, NY, [2]Scarsdale, NY

Disclosures: Yihua Zhou: None; Atsushi Tanaka: None; Ronald Hendrickson: None; Julia Wang: None; Michael H. A. Roehrl: None

Background: Formalin fixation and paraffin embedding (FFPE) procedures are cost-efficient and widely adopted methods for preserving human tissue biospecimens. Unlocking FFPE samples by ultra-high resolution Fourier-transform mass spectrometry for deep proteome profiling will open unmatched resources in biomarker discovery. Due to chemical cross-linking and low solubility in usual protein lysis buffers, there is still a lack of robust and reproducible FFPE proteomics standard procedures for sample preparation that can reliably retrieve total tissue-resident proteomes from clinical FFPE specimens.

Design: To improve protein solubility, which will result in broader proteome coverage, we chose a lysis buffer containing the strong ionic detergent sodium dodecyl sulfate (SDS) for protein extraction from FFPE tissues. We then compared three different methods, i.e, in solution digestion, in gel digestion, and the new Suspension Trap (S-Trap, Protifi) method, to find the most effective procedure for liquid chromatography mass spectrometric analysis. For each method, we used the same 8 FFPE samples from primary colorectal adenocarcinoma. All samples were double digested with trypsin and Lys-C. In solution digestion was performed with Pierce detergent removal spin columns to remove residual SDS before C18 desalting. Final peptide amounts were measured by the Pierce quantitative colorimetric peptide assay. We compared average peptides recovery rates between the three methods.

Results: We compared three mass spectrometric extraction methods by using 100 µg FFPE protein inputs and measuring peptide digest concentrations prior to LC-MS injection. Average peptide recovery rates of in solution, in gel digestion, and S-Trap methods, were 9.1%, 9.5% and 93.5%, respectively.

Conclusions: In comparison with traditional in solution and in gel digestion methods, the new S-Trap digestion significantly outperformed the other methods in FFPE samples. Mandatory SDS removal prior to LC-MS injection significantly limits in solution digestion peptide recovery. The S-Trap protocol requires slightly more time than typical in solution or in gel digestion, but provides the flexibility to use powerful SDS detergent solubilization for maximally deep proteome representation in mass spectrometric sample preparation.